

**Construction and Dynamics of Knotted Soft Matter
Systems**

by

Jack Binysh

Thesis

Submitted to the University of Warwick

for the degree of

Doctor of Philosophy

Centre for Complexity Science

....

Contents

Acknowledgments	ii
Declarations	iii
Abstract	iv
Chapter 1 An Introduction to Knotted Fields	1
1.1 Kelvin's vortex atom	1
1.2 Modern knotted fields: Fluids	5
1.2.1 Calugareanu's Theorem, Real fluids	7
1.2.2 Fluids as a case study	8
1.3 Modern knotted fields: Liquid Crystals	9
1.3.1 A brief introduction to liquid crystals	10
1.3.2 Homotopy theory of knotted disclinations and Pontryagin-Thom surfaces	14
1.3.3 Beyond disclination lines	17
1.4 Modern knotted fields: Excitable Media	25
1.5 Structure of this Thesis	34

Acknowledgments

Yes Mum I've finished my PhD now. No, I don't know what I'm going to do next.

Declarations

Replace this text with a declaration of the extent of the original work, collaboration, other published material etc. You can use any L^AT_EX constructs.

Abstract

Chapter 1

An Introduction to Knotted Fields

1.1 Kelvin's vortex atom

The original, and perhaps most familiar, example of a knotted field is the smoke ring. Easily made by cutting a circular hole in a rectangular box, then replacing the opposite side entirely with a sheet of rubber, “a blow on this flexible side causes a circular vortex ring to shoot out from the hole on the other side” [Thomson, 1867]. In 1867, exactly this demonstration was shown to Lord Kelvin by Peter Guthrie Tait. What is generated is a tightly circulating tube of air, closed into a ring, which propagates stably across the room, rebounding elastically from walls and even other vortex rings (of course to see the ring one first needs to fill the box with smoke, perhaps using dry ice or “a small quantity of muriatic acid” [Thomson, 1867]). At the time, the microscopic nature of atoms was still under debate, and the stability of the rings, a consequence of Helmholtz’s laws of vortex motion in an ideal fluid [Helmholtz, 1858] (translated into English by Tait), coupled with their elasticity and capacity for internal vibration [Laan, 2012; Lomanaco, 1996] prompted Kelvin to suggest that “Helmholtz’s rings are the only true atoms” [Thomson, 1867]. Kelvin hypothesised that such rings, embedded in a “perfect homogenous liquid”¹, and “linked together or ... knotted in any manner” might form the microscopic basis of matter [Thomson, 1867].

Kelvin’s “vortex atom” encountered difficulties in its mathematical content, its falsifiability, and a lack of contemporary experimental support [Laan, 2012]. How-

¹Kelvin did not actually specify whether this fluid was the same as the ‘ether’ hypothesised to transmit electromagnetic waves [Laan, 2012].

a

GLENLAIR
DALBEATTIE,
Nov. 13, 1867.

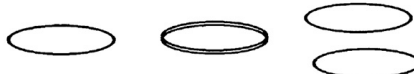
Dear Tait

If you have any spare copies of your translation of Helmholtz on "Water Twists" I should be obliged if you could send me one.

I set [sic] the Helmholtz dogma to the Senate House in '66, and got it very nearly done by some men, completely as to the calculation, nearly as to the interpretation.

Thomson has set himself to spin the chains of destiny out of a fluid plenum as M. Scott set an eminent person to spin ropes from the sea sand, and I saw you had put your calculus in it too. May both prosper and disentangle your formulae in proportion as you entangle your worbles. But I fear the simplest indivisible whirl is either two embracing worbles or a worble embracing itself.

For a simple closed worble may be easily split and the parts separated



but two embracing worbles preserve each others solidarity thus



though each may split into many, every one of the one set must embrace every one of the other. So does a knotted one.



yours truly

J. CLERK MAXWELL

c

422.] VECTOR-POTENTIAL OF A CLOSED CURVE. 41

to be intertwined alternately in opposite directions, so that they are inseparably linked together though the value of the integral is zero. See Fig. 4.

It was the discovery by Gauss of this very integral, expressing the work done on a magnetic pole while describing a closed curve in presence of a closed electric current, and indicating the geometrical connexion between the two closed curves, that led him to lament the small progress made in the Geometry of Position since the time of Leibnitz, Euler and Vandermonde. We have now, however, some progress to report, chiefly due to Riemann, Helmholtz and Listing.

422.] Let us now investigate the result of integrating with respect to σ round the closed curve.

One of the terms of Π in equation (7) is

$$\frac{\xi - \eta}{r^3} \frac{dx}{ds} \frac{dz}{ds} = \frac{d\eta}{ds} \frac{d}{d\xi} \left(\frac{1}{r} dz \right). \quad (8)$$

If we now write for brevity

$$F = \int \frac{1}{r} \frac{dx}{ds} ds, \quad G = \int \frac{1}{r} \frac{dy}{ds} ds, \quad H = \int \frac{1}{r} \frac{dz}{ds} ds, \quad (9)$$

the integrals being taken once round the closed curve s , this term of Π may be written

$$\frac{d\eta}{ds} \frac{d^2H}{d\xi ds},$$

and the corresponding term of Π will be

$$\frac{d\eta}{ds} \frac{dH}{d\xi}.$$

Collecting all the terms of Π , we may now write

$$-\frac{d\omega}{ds} = -\int \Pi ds = \left(\frac{dH}{d\xi} - \frac{dG}{d\zeta} \right) \frac{d\xi}{ds} + \left(\frac{dF}{d\zeta} - \frac{dH}{d\eta} \right) \frac{d\eta}{ds} + \left(\frac{dG}{d\xi} - \frac{dF}{d\eta} \right) \frac{d\xi}{ds}. \quad (10)$$

This quantity is evidently the rate of decrement of ω , the magnetic potential, in passing along the curve σ , or in other words, it is the magnetic force in the direction of $d\sigma$.

By assuming $d\sigma$ successively in the direction of the axes of x , y and z , we obtain for the values of the components of the magnetic force

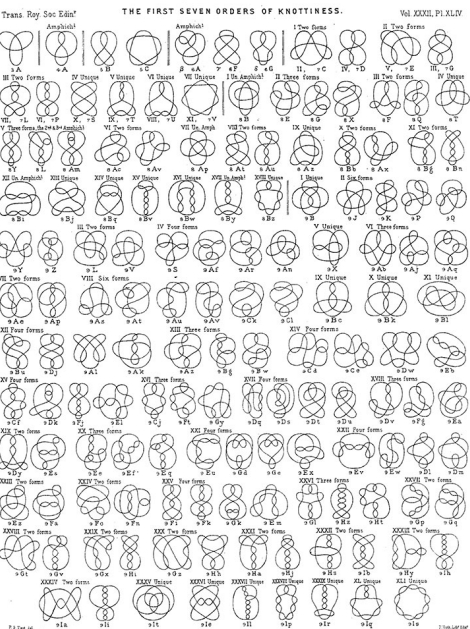
b

two closed curves and/or the distance between them and of $L M N$, $\lambda \mu \nu$, and $L M N$ are the direction cosines of $ds = dx + dy + dz$ respectively,
then $\int ds = \sqrt{\left(\frac{dx}{ds} \right)^2 + \left(\frac{dy}{ds} \right)^2 + \left(\frac{dz}{ds} \right)^2}$
 $= \int ds = \sqrt{\left(1 - \frac{dx}{ds} \right) \left(1 - \frac{dy}{ds} \right) \left(1 - \frac{dz}{ds} \right)} = \sqrt{\left(r \cos \theta \right)^2}$
 $= 4\pi n$
the integration being extended round both curves and n being the algebraic number of times that one curve embraces the other in the same direction.
If the curves are not linked together $n = 0$ but if $n = 0$ the curves are not necessarily independent.



In fig 1 the two closed curves are inseparable but $n = 0$. In fig 2 the 3 closed curves are inseparable but $n = 0$ for every pair of them. Fig 3 is the simplest ~~and~~ knot on a simply curve. The simplest equation I can find for it is $r = b + a \cos^2 \theta$ $z = c \sin \frac{\theta}{2}$ when c is $-ve$ as in the figure the knot is right-handed when c is $+ve$ as left-handed, its right-handed knot cannot be changed into a left-handed one

d



ever its content, summarised as “*Physics = Geometry*” in Ref. [Lomanaco, 1996], was compelling, and apparently motivated Tait, in “consideration of the forms of knots by Sir W. Thomson’s (Lord Kelvin) Theory of Vortex Atoms”, to construct the first systematic tables of knots in 1876–1885, shown in Figure 1.1 [Tait, 1876, 1883, 1884]. Tait’s articles, alongside a “very remarkable essay by Listing ... and an acute remark made by Gauss ... with some comments on it by Clerk-Maxwell” [Tait, 1876] form the initial studies in what is now the mathematical field of Knot Theory [Lickorish, 1997]. Maxwell himself, although not an active contributor to vortex atom theory, had a clear interest in the ideas, encouraging Tait and Kelvin to “prosper and disentangle your formulae in proportion as you entangle your worbles” (Figure 1.1). Indeed the “comments by Clerk-Maxwell” referred to by Tait are in fact Maxwell’s rederivation of Gauss’s Linking number, as presented in his *A Treatise on Electricity and Magnetism* [Maxwell, 1873] in 1873, about which we will have much more to say in §§??.

Despite forming the starting point for modern knot theory, the knotted structures above are quite different to those found in your shoelaces, or in the world of art and design outside the physics department. Rather than a single knotted curve, we have a continuous fluid in whose structure the knot is encoded, and from which dynamical properties of the knot (its motion, stability, a spectrum of vibrational modes etc.) may be derived. More precisely, we have a concentrated tube of vorticity in the fluid, tied into the shape of a knot. Helmholtz’s laws of vortex motion demonstrated that, in a perfect (frictionless) fluid this tube of vorticity was ‘frozen in’ to the fluid, unable to dissipate or cross itself. In an idealised vortex atom, the radius of this tube would tend to zero, with the vorticity contained inside becoming infinite, and we would have a singular linelike structure, tied into a knot and embedded into a continuous three dimensional medium. This structure is our first example of what is called a *knotted field*. There is no strict definition of what constitutes of a knotted field, but a sensible effective one is that they are physical fields containing knotted, linked, or otherwise topologically interesting structure, and that this structure has some interplay with the behaviour of the whole field. As we shall see, such fields are not certainly not confined to fluids.

The disconnect between a knotted curve and a knotted field is reflected in Tait’s work, which mentions Kelvin’s Vortex Atoms briefly as motivation, but focuses in substance on “*the investigation of the essentially different modes of joining points in a plane*” [Tait, 1876]. As knot theory developed, its initial connections to hydrodynamics and electromagnetism were further abandoned. One also notes that despite the wonderful knot tables produced by Tait (figure 1.1) and the reliance of

vortex atom theory on knotted and linked vortices, there is no mention above of any experimental evidence of vortices tied in nontrivial knots.

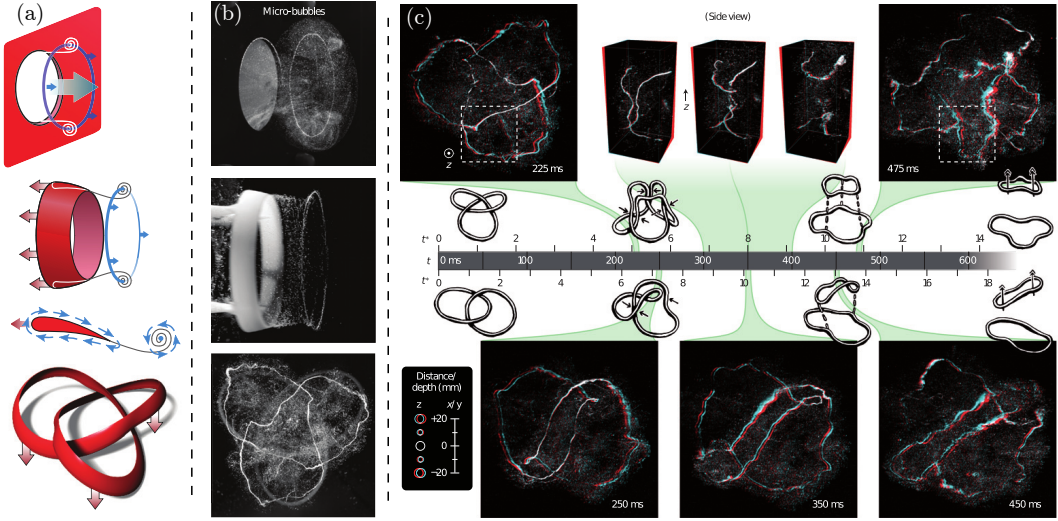


Figure 1.2: The first experimental construction of knotted vortices, in 2013. (a) Experimental methods for making knotted vortices. The hydrofoil (bottom three panels) is most successful. (b) Vortices produced in water from the designs of figure (a). Microbubbles injected into the water track the vortex. (c) Timelines showing the evolution of a trefoil knot (top) and Hopf link (bottom) in three dimensions. In contrast to ideal fluids, we see progressive reconnections and simplification of the links. Figure reproduced (modified) from [Kleckner and Irvine, 2013].

The first experimental construction of nontrivial knotted fluid vortices came 140 years after their initial theoretical investigation, from the Irvine lab in 2013 — we show in figure 1.2 several remarkable figures reproduced from Ref. [Kleckner and Irvine, 2013], in which Kleckner et al. tied a single vortex in water into a trefoil knot, the simplest nontrivial knot, as well as linking two vortex loops together (Kelvin’s proposed model for a Sodium atom), before tracking their full three-dimensional evolution. Ref. [Kleckner and Irvine, 2013] is a notable example of a more general trend; over the past ~ 10 years knotted fields have gone from being purely theoretical constructions to being experimentally realisable in a number of systems, and though originally conceived of in fluid dynamics, modern applications are not limited to this context; they have been realised as nodal lines of optical beams [Dennis et al., 2010], as disclinations in nematic liquid crystals and as spinor Bose-Einstein condensates [Tkalec et al., 2011; Tasinkevych et al., 2014; Čopar et al., 2015]. In the following sections we will review the state of modern experiment and theory on knotted fields, beginning with fluids and superfluids, in some sense the most developed case, before moving on to parallel developments in liquid crystals and

excitable media, which directly underlie the work in §§?? and §§?? in this Thesis; these examples are certainly not exhaustive, and focus on ‘Soft Matter’ systems, a point we shall discuss at the end of the chapter. We shall see that the subject has broadened considerably since Kelvin’s atoms and his contemporaries’ study of fluids. There will be a commonality of ideas between the different disciplines mentioned above, but also genuine differences.

TODO: SPINORS?

1.2 Modern knotted fields: Fluids

With the decline of Kelvin’s vortex atom theory and the development of knot theory away from its hydrodynamic origins, a resurgence of interest in knotted fields might be dated to the years 1958–1969, with Moreau and Moffatt’s seminal papers on Helicity in ideal fluids [Moreau, 1961; Moffatt, 1969], preceded by analogous results in magnetohydrodynamics by Woltjer [Woltjer, 1958]. Focusing on the ideal fluid, both Moreau and Moffatt independently demonstrated that the Helicity

$$\mathcal{H} = \int \mathbf{u} \cdot \boldsymbol{\omega} \, d^3\mathbf{r}, \quad (1.1)$$

where $\mathbf{u}(\mathbf{r}, t)$ is the fluid velocity and $\boldsymbol{\omega} = \nabla \times \mathbf{u}$ is the vorticity [Saffman, 1992], is conserved under the Euler equations of ideal flow. Moffatt in particular gave this invariant a topological interpretation: it measures the linking of vortex tubes within the fluid. Given a fluid where ω is concentrated along discrete sets of curves C_i , Moffat showed that

$$\mathcal{H} = \sum_{i,j,i \neq j} Lk(C_i, C_j) \Gamma_i \Gamma_j \quad (1.2)$$

where Γ_i is the vorticity flux of along curve C_i , and $Lk(C_i, C_j)$ is the Gauss Linking number between curves C_i, C_j (this interpretation of Helicity actually extends to the case where the vorticity is not concentrated along a finite set of curves, but is distributed throughout the fluid [V. I. Arnold, 1999]). Figure 1.3 shows several examples of vortex tubes with different linking numbers and hence helicities. Seen in this light, the conservation of Helicity is a direct consequence of Helmholtz’s laws of vortex motion, and is equivalent to the statement that initially linked vortex tubes remain so; in some sense it is remarkable that the result was not known to Kelvin and Maxwell.

When vorticity is not concentrated along a singular curve but distributed in a thin vortex tube, there is additional internal structure — one imagines a knotted ribbon (Figure 1.4(a)), or rubber bicycle tyre (Figure 1.4(b)). Flux lines may wind

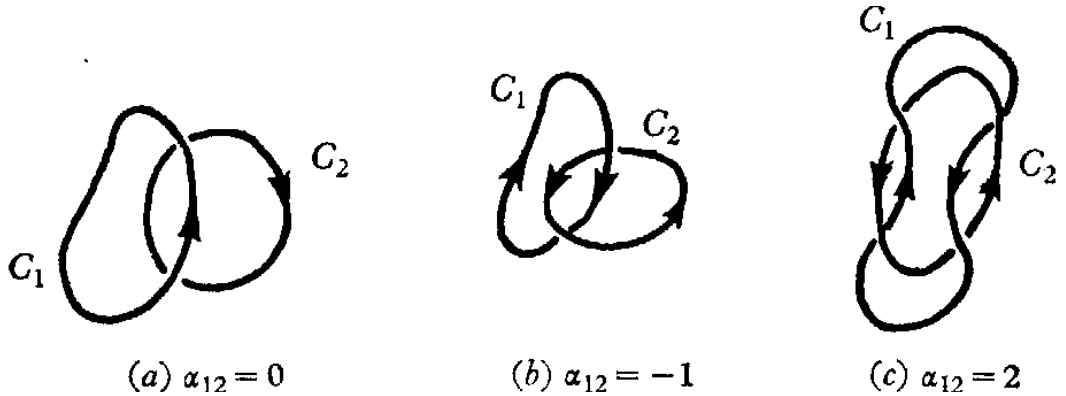


Figure 1.3: Three examples of links with different linking numbers. In the figure, $Lk(C_i, C_j)$ is denoted α_{ij} . Figure reproduced from [Moffatt, 1969].

around the centre-line of this tube as in Figure 1.4(b), endowing it with a second linking number, the Self-Linking number, which measures the linking of any flux line with the curve centre-line, or equivalently the number of rotations any flux line makes as we traverse the centre-line once. Incorporating this structure into the

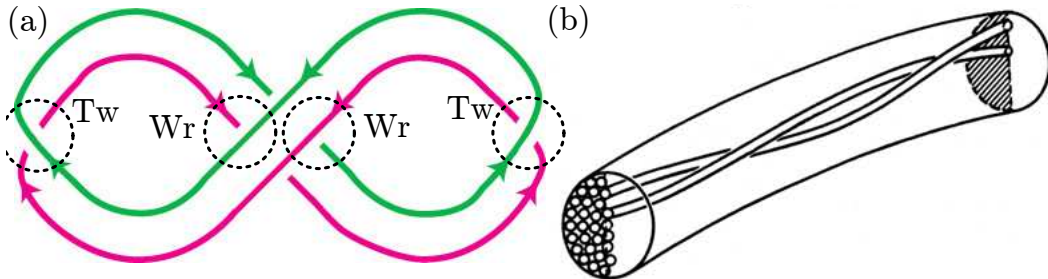


Figure 1.4: A curve with internal structure: ribbons and tubes. (a) A ribbon, defined by a centre-line (pink, say) and a second offset curve (green). The diagram is a projection of a three-dimensional structure, and each crossing may be annotated as either a twist or writhe crossing, depending on its local (green across pink, no pink across pink) or nonlocal (green across pink + pink across pink) nature. The total count gives a self linking number for the ribbon; see eq. 1.4. (b) A twisted tube, in which one particular ‘filament’ may be arbitrarily chosen to define a ribbon. This is the situation in vortex tubes. Figures reproduced (modified) from [Dennis and Hannay, 2005; Moffatt and Ricca, 1992].

helicity count we find [Moffatt and Ricca, 1992]

$$\mathcal{H} = \sum_{i,j, i \neq j} Lk(C_i, C_j) \Gamma_i \Gamma_j + \sum_i \Gamma_i^2 SL(C_i) \quad (1.3)$$

where $SL(C_i)$ denotes the self linking of each curve C_i with its implicitly assumed

ribbon.

1.2.1 Calugareanu's Theorem, Real fluids

Given a ribbon diagram like figure 1.4(a), the self linking number of may be further decomposed as

$$SL = Tw + Wr. \quad (1.4)$$

The first term, the twist Tw , counts the local crossings of the ribbon over its centre-line. The second term, the writhe Wr , counts non-local crossings of the ribbon over distant parts of the centre line. In figure 1.4 each crossing of the ribbon over its centre-line is annotated with the nature of its contribution. Note that the Wr count is actually independent of the choice of ribbon. For different diagrams of the same knotted ribbon each of these contributions varies, but their sum SL does not. Averaging over also possible diagrams, i.e. all possible projections of the genuine three-dimensional curve, one obtains integral formulae for twist and writhe, and in this form the result eq. 1.4 was first discovered by Georges Calugareanu [Călugăreanu, 1959, 1961] (the interpretation of it given above is however due to Ref. [Dennis and Hannay, 2005]). Calagareanu's Theorem is an important and influential result, finding application in Mathematics, Physics, Biology and beyond. It is of potential relevance whenever one studies the properties of a curve with some internal structure, and so it naturally appears frequently in the study of knotted fields. It will play a role in the curve dynamics studied in §§??, in conservation laws encountered in §§?? and, in its close connection to Maxwell and Gauss's work on linking numbers and electromagnetism, in §§?? as well. For the purposes of the current discussion it enables us to speak of *writhe* helicity and *twist* helicity, two separate contributions to the total helicity count.

In a real (viscous) fluid, helicity is not *a priori* conserved. The question of whether it is in practice, and the mechanism of its dissipation, are areas of active research and motivation for the experiments shown in Figure 1.2 [Kleckner and Irvine, 2013]. The reconnections shown in figure 1.2 suggest that helicity is not conserved, however experiments tracking its evolution in detail [Kleckner and Irvine, 2013; Scheeler et al., 2014, 2016] find that this is not the case. Instead, reconnections transfer the initial linking of curves into self linking (c.f. eq. 1.3) , preserving total helicity to a remarkable extent. More precisely, what is conserved is the sum $Lk + Wr$, with the helicity in Lk being transferred to Wr at a reconnection; the twist helicity Tw is dissipated by viscosity. Figure 1.5 shows the experimental tracking of each contribution to total helicity as a vortex ring in water evolves,

demonstrating this to be the case.

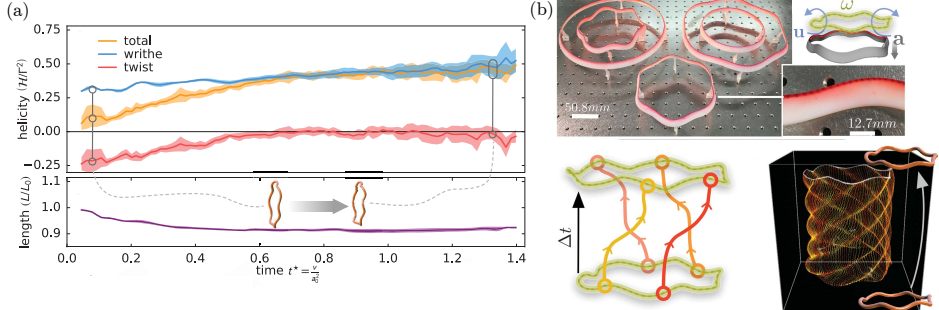


Figure 1.5: Evolution of helicity in a viscous fluid. (a) The three contributions to helicity are experimentally tracked as a vortex ring evolves. Twist helicity dissipates to zero, but writhe helicity is conserved (in fact, generated [Scheeler et al., 2016]). (b) Flow field resolution within the vortex core is enabled by impregnating an aerofoil with separated blobs of dye, which are traced over time. Figure reproduced (modified) from Ref. Scheeler et al. [2016].

1.2.2 Fluids as a case study

The hydrodynamic (and magnetohydrodynamic) story of knotted fields is well developed. We have given a sketch, but the reader is invited to find more detail in reviews such as Refs. [Moffatt, 2014; Irvine, 2018]. Outside of hydrodynamics the above discussion acts as a template for what one might expect in knotted fields more generally; a test case which other systems may be compared to and contrasted against. In particular, linking and self-linking of structure occur in a variety of contexts, and in an analogy to (1.3) one might seek to connect them to conserved quantities, and use them to understand the dynamics of the entire system under study. To give a brief example of system for which this template is fruitful consider superfluids, close cousins of normal fluids described by a complex scalar field $\psi = |\psi|e^{i\phi}$ (Figure 1.6(a)) evolving via the non-linear Schrödinger equation [Kleckner and Irvine, 2013]. Here vortices are given by singular lines where the circle-valued phase field ϕ is undefined, and about which it winds by 2π . As in fluids, one may define some notion of helicity (although its precise form is more ambiguous than is the case in fluids [?]), initialise knotted vortices and study their evolution (figure 1.6(b)) [Kleckner and Irvine, 2013; Scheeler et al., 2014]. The helicity evolution turns out to be remarkably similar to that of real fluids [Kleckner and Irvine, 2013; Scheeler et al., 2014]; reconnections occur in a manner similar to those found in real fluids, and they preserve the combination $Lk + Wr$.

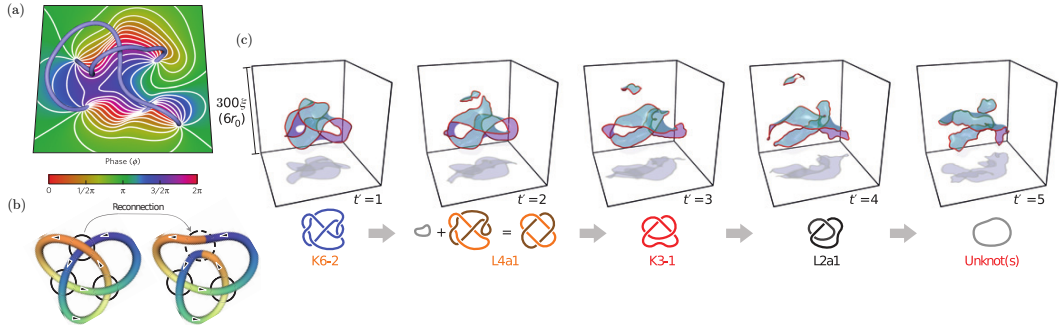


Figure 1.6: Evolution of superfluid vortex knots. (a) Cross section through a superfluid vortex knot (light blue curve), showing the phase field ϕ winding by 2π about the vortex. (b) A schematic illustration of a reconnection. Colour is for visualisation only; note the splicing. (c) An example untying of a superfluid link into a collection of unknots by progressive recombinations. Blue surfaces spanning the knot are surfaces of constant phase. A schematic of the untying process is shown below.

However, it is not the case that knotted fields in all other systems may be understood simply through the lens of fluids. In the following section we turn to the second experimental system with which substantial work on knotted fields has been done, the nematic liquid crystal cells of Refs. [Tkalec et al., 2011; Tasinkevych et al., 2014; Čopar et al., 2015]. There will be some crossover with the discussion above, but also genuine differences, especially in the theoretical constructions involved, which are of a quite different character.

1.3 Modern knotted fields: Liquid Crystals

A second experimentally constructed knotted field is shown in figure 1.7. It is quite different to that of figure 1.2. By including microscopic colloids a few μm wide into a thin cell of nematic liquid crystal, experimentalists [Tkalec et al., 2011; Tasinkevych et al., 2014; Čopar et al., 2015] are able to force the appearance of defect lines in the material. These defects may then be manipulated with lazer tweezers, and by weaving them about an array of colloids, a knotted field encoding any type of knot or link can be constructed; unlike the fluid vortices above, these structures are stable, able to be experimentally probed in some detail. This system provides a testbed for series of new ideas about knotted fields described below, but first we step back a moment and provide a brief description of what liquid crystals, defects and colloids etc. actually are.

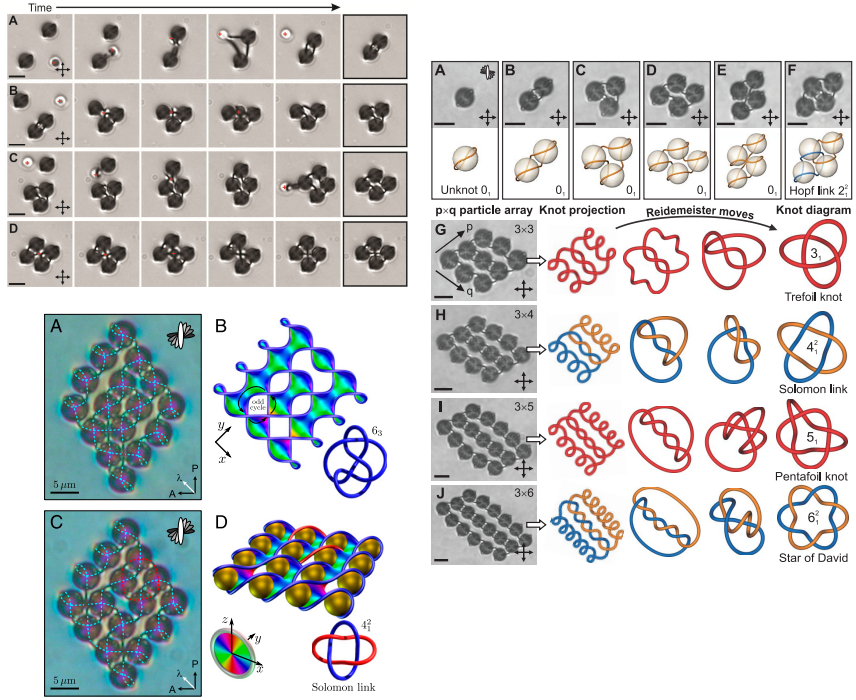


Figure 1.7: hi

1.3.1 A brief introduction to liquid crystals

Liquid crystals are a class of materials which possess properties associated to both liquids and solids [P. G. de Gennes, 1996]. In their most common form, the nematic phase, they show no positional order, and flow like a liquid. However, they do show orientational order: if one attempts to twist a portion of the liquid crystal it will respond elastically, as a solid would². The microscopic basis for this behaviour comes from the type of molecules which comprise nematics, two examples of which are shown in Figure 1.8; they are typically thin rods which locally align themselves along some common axis without taking on any sort of crystalline positional order. In continuum theories this orientational order is described by a spatially varying unit vector field \mathbf{n} , called the director, which represents an average local molecular orientation, as shown in Figure 1.8 (c).

The theory of their elastic distortions contains much interesting geometry which we will return to in §1.3.3, but for an understanding of figure 1.7 we instead focus on a celebrated feature of nematics [Frank, 1958], their topological defects. If one shines polarised light through a thin slice of nematic placed between crossed

²This is remarkable: imagine your surprise if, upon attempting to stir your coffee, you found it fiercely resisted your attempts to turn the spoon, but was nevertheless happy to be poured down the sink.

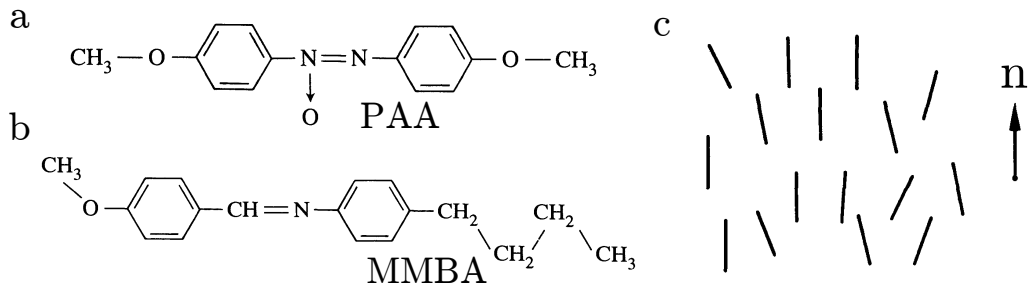


Figure 1.8: (a), (b) Two examples of molecules which can form a nematic liquid crystalline phase. (a) p-azoxyanisole (PAA) forms a nematic between 116–135 °C at atmospheric pressure. (b) N-p-methoxybenzylidene-p-butylanilinie (MBBA) forms a nematic between 20–47 °C. (c) A schematic of local alignment, with the director \mathbf{n} giving a direction averaged over microscopic lengthscales. Figures reproduced (modified) from [P. G. de Gennes, 1996]

polarisers, they will observe something like figure 1.9 (a), a Schlieren texture [P. G. de Gennes, 1996]. Places in the sample where the director \mathbf{n} is aligned with one of the two polariser directions H and V do not transmit light, leading to the dark brushes observed. One immediately notes points where the brushes meet, sometimes with two brushes leading into a point, sometimes four. What is the structure of the director at these points? The confluence of dark brushes implies that, in a small circle around these points, the director winds, and that at the point itself we cannot consistently define \mathbf{n} ; these points are topological defects, places where the order breaks down. Traversing such a circle around a point with two brushes, the director is aligned with each of H and V only once; in other words it makes only half a turn in a full circle around the defect. This observation is enough to establish that the director \mathbf{n} must in fact be non-orientable; it should not be thought of as a vector field, but as a line field, for which $\mathbf{n} \sim -\mathbf{n}$.

In figure 1.9 (b)–(e) we show qualitative configurations of the director around these defects, with their associated Schlieren texture brushes. In (b) and (e) we have four brushes, and a line field which can be oriented; to emphasise this fact we have decorated the line field with one of the two possible choices of arrowheads. Figures (c) and (d) correspond to the non-orientable two brush case; here one cannot consistently assign arrowheads to the rods (it is worth trying to imagine doing so). Note that from a single image such as figure 1.9(a), we cannot distinguish defects winding in a right handed sense (+, in the figure) from left handed by counting brushes. In two dimensions these defects, also called disclinations or *disinclinations* [Frank, 1958], are points, but in three dimensions they are lines, transverse cross

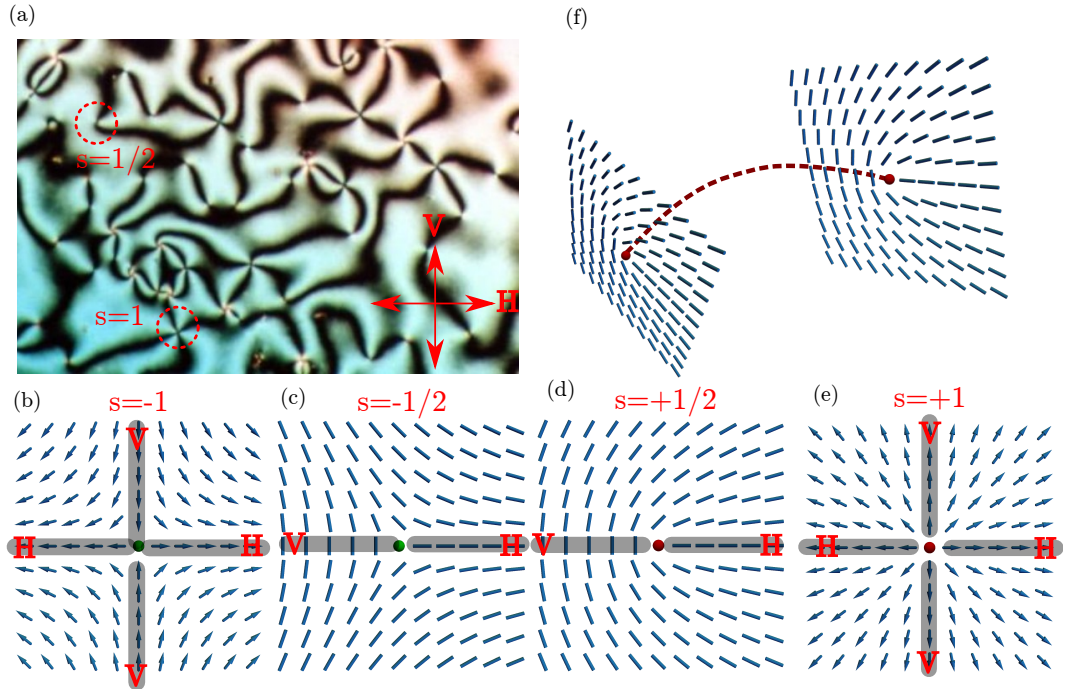


Figure 1.9: Topological defects in liquid crystals. (a) A Schlieren texture, with crossed polarizer directions overlaid, and defects of winding number (s) $\frac{1}{2}$ and 1 highlighted (one cannot distinguish \pm from the picture alone). (b)–(e) Topologically accurate director configurations around defects of winding number (s) $\pm\frac{1}{2}$, ± 1 , with the Schlieren dark brushes overlaid. For ± 1 defects it is possible to orient the director, and we have made one of the two possible choices of arrowheads. (f) Schematic of a disclination line in a three-dimensional nematic sample, with two cross sections showing local structure. Locally, there is only one type of disclination ($\pi_1(\mathbb{R}P^2) \approx \mathbb{Z}_2$) so a winding s is not given.

sections of which have local profiles resembling the two dimensional case; a schematic illustration is shown in Figure 1.9(f). As with fluid vortices, these disclination lines may be knotted and linked together, and the rotation of the local profile along the disclination (see the cross sections in Figure 1.9(f)) provides internal structure giving rise to self linking.

Experiments on knotted disclination lines

We now return to the experiments of Refs [Tkalec et al., 2011; Tasinkevych et al., 2014; Čopar et al., 2015]. In contrast to situation in fluids, one of the major advantages of working with liquid crystal disclinations is the control experimentalists have over them. By including microscopic silica spherical colloids ($4.72 \mu\text{m}$ diameter in figure 1.7) into a sample of liquid crystal with specific surface anchoring conditions, experimentalists may frustrate alignment of the director \mathbf{n} in a controlled fashion, necessitating the appearance of disclination lines. For example, in a thin cell of liquid crystal treated to promote uniform alignment of \mathbf{n} within the sample, the inclusion of a colloid with normal anchoring conditions forces the appearance of a defect line around it to cancel the colloid's topological charge (it effectively acts as a point defect) and allow \mathbf{n} to relax to uniform at large distances. Two such "Saturn's ring" configurations may be seen in the first frame of figure 1.7(a). Once generated, these disclinations, as well as the colloids they wrap around, may be further manipulated using lazer tweezers [Tkalec et al., 2011], as shown in the remainder of figure 1.7(a). When two of these colloids are brought together the disclinations, either spontaneously or induced by the tweezers, fuse together (Figure 1.7(a), top row). Assembling an array of these colloids and weaving the disclination lines around them, the setup of Refs. [Tkalec et al., 2011; Tasinkevych et al., 2014; Čopar et al., 2015] allows targeted construction of any knot or link; examples of some possible link topologies are shown in Figure 1.7 (b). This system strikingly illustrates that knotted fields have more structure than a single knotted curve; the curve organises the entire field (in this case the director \mathbf{n}) around it. Figure 1.7(c) shows the knotted liquid crystal coloured by whether the director is twisting in a right or left handed sense. We see that the disclinations separate the liquid crystal into alternately right and left handed regions. In fact this division allows construction of a surface spanning the disclinations called the Pontryagin-Thom (PT) surface [Chen et al., 2013; Chen, 2012], shown as the coloured surfaces in figure 1.7(c), which classifies the topology of this liquid crystal texture; we shall return to it in a moment.

Let us compare the phenomena seen here to §1.2. In contrast to fluid vortices,

it is experimentally possible to stabilise liquid crystal disclinations with colloids. This fact alone leads to many differences in the character of theoretical work on them. In the absence of the stabilising colloids, the disclinations will shrink under effective line tension and undergo reconnections, however there is relatively little theoretical work on possible conservation laws analogous to eq. (1.3) or on the structure of these reconnections, although some results do exist ?. In this sense the dynamics of these knotted fields is less understood than is the case in fluids. It turns out, however, that there is much to be understood even about the statics of knotted liquid crystal fields. Loosely, this may be understood by observing that in a two dimensional fluid there is only one type of vortex, topologically speaking. In a slice of liquid crystal, however, we saw there were many types, indexed by the winding of the director. What of liquid crystal textures in three dimensions? More specifically, given the knotted disclinations shown in figure 1.7, are the liquid crystal textures corresponding to them unique, or are there many inequivalent possibilites? Questions like these have a long history in liquid crystal physics which, coupled with the difference in experimental possibilites we saw above, makes some split between the character of work on knotted fields in fluids and that in liquid crystals expected.

1.3.2 Homotopy theory of knotted disclinations and Pontryagin-Thom surfaces

The traditional method of understanding liquid crystal textures containing defects is to place a measuring surface around a defect and study the possible textures on this surface, i.e. the different classes of map from the measuring surface to the space of possible values the order takes. Maps are equivalent when a continuous deformation, called a homotopy, exists between them, and as such this framework is known as the homotopy theory of defects [Mermin, 1979; Alexander et al., 2012]. For point defects in a two-dimensional slice of nematic, this is what we did above, using a circle as our measuring surface. There, the space of possible directions \mathbf{n} can point in is $S^1/\{x \sim -x\}$, the circle with antipodal points identified, also called the real projective line \mathbb{RP}^1 . Thus the different classes of texture are reduced to the classification of maps $\mathbf{n} : S^1 \rightarrow \mathbb{RP}^1$. Actually computing these classes is the work of Algebraic Topology [Hatcher, 2002], in which maps of a sphere S^n into a space X are termed the homotopy groups $\pi_n(X)$. It is found that $\pi_1(\mathbb{RP}^1) \approx \mathbb{Z}$ and thus there are infinitely many types of point defect in two dimensions as far as the traditional form of the theory is concerned; we show the four simplest in figure 1.9 but the index extends infinitely in both + and – senses. In three dimensions, the director takes values in $S^2/\{x \sim -x\}$, the sphere with antipodal points identified, also called

the real projective plane \mathbb{RP}^2 . Encircling a disclination line with a measuring loop as shown in Figure 1.10, one finds $\pi_1(\mathbb{RP}^2) \approx \mathbb{Z}_2$, and thus there are precisely two distinct types of disclination³.

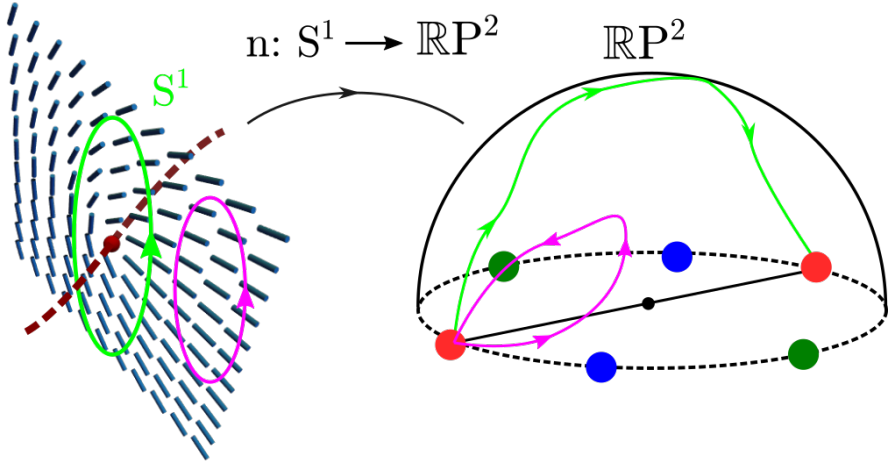


Figure 1.10: Application of the homotopy theory of defects to disclination lines. We place a measuring loop (green) around a disclination line (red curve). We then regard the director \mathbf{n} (blue cylinders) as a map from this loop to the order space of the director; in this case \mathbb{RP}^2 , modelled here as a hemisphere with equatorial points identified (pairs of red, blue, green dots indicate this identification). Homotopy theory then classifies this map as an element of $\pi_1(\mathbb{RP}^2) \approx \mathbb{Z}_2$, in the case the single nontrivial element. If our measuring loop misses the disclination (purple) it traces a trivial path in \mathbb{RP}^2 .

A limitation of this approach is that, in only considering the texture on a specific measuring surface (in practice a sphere of some dimension) it discards information about the rest of the texture, which leads to ambiguities when considering multiple defects or more complex structures such as knotted and linked disclinations [Alexander et al., 2012; Machon, 2016; Machon and Alexander, 2014, 2016a]. A more recent, global approach [Machon, 2016; Machon and Alexander, 2014, 2016a] does not fix a measuring surface, but instead classifies maps into \mathbb{RP}^2 where the domain is the entire liquid crystal sample M minus some set of (possibly knotted and linked) disclination lines L . The result is that the homotopy classes of the director are given by

$$[M - L, \mathbb{RP}^2] \approx H_1(\Sigma(L); \mathbb{Z}) / \{x \sim -x\} \quad (1.5)$$

³One understands this difference by allowing the director in figures 1.9 (b) and (c) to buckle out of the plane of the paper, reducing these textures to the trivial one. This “escape in the third dimension” causes \mathbb{Z} to undergo a mod 2 reduction.

where $\Sigma(L)$ is the branched double cover of the link complement (its appearance in the result is a consequence of director non-orientability), and $H_1(\Sigma(L); \mathbb{Z})$ is its first homology group. Without going into the details of this result, it is clear that these homotopy classes are far richer than the traditional classification scheme for disclinations would suggest, and that they depend strongly on the knot or link under consideration. To illustrate this point, in figure 1.11 we reproduce a ‘periodic table’ of possible textures for (p, q) torus links from Ref. [Machon, 2016]. Taking the simplest example from this table we see that for the Hopf Link, consisting of two curves passing through each other once and given by $(p, q) = (2, 2)$, there are exactly two nonhomotopic textures. Returning to the knots shown in figure 1.7, for each knot there may be multiple nonhomotopic textures, and the knot diagram alone does not tell us which has actually been made. How should we extract this information, and visualise distinct textures? In figure 1.9 simple pictures of the director in the vicinity of a defect prove informative, but the same cannot be said of a swarm of sticks in three dimensions.

$p \setminus q$	2	3	4	5	6	7	8	9	10	11	12	13	14	15	16	17	18	19	20
2	2	3	4	5	6	7	8	9	10	11	12	13	14	15	16	17	18	19	20
3	3	2^2	3	1	Z^2	1	3	2^2	3	1	Z^2	1	3	2^2	3	1	Z^2	1	3
4	4	3	$2 \times Z^2$	5	12	7	$4 \times Z^2$	9	20	11	$6 \times Z^2$	13	28	15	$8 \times Z^2$	17	36	19	$10 \times Z^2$
5	5	1	5	2^4	5	1	5	1	Z^4	1	5	1	5	2^4	5	1	5	1	Z^4
6	6	Z^2	12	5	$2 \times Z^4$	7	24	$3 \times Z^2$	30	11	$4 \times Z^4$	13	42	$5 \times Z^2$	48	17	$6 \times Z^4$	19	60
7	7	1	7	1	7	2^6	7	1	7	1	7	1	Z^6	1	7	1	7	1	7
8	8	3	$4 \times Z^2$	5	24	7	$2 \times Z^6$	9	40	11	$12 \times Z^2$	13	56	15	$4 \times Z^6$	17	72	19	$20 \times Z^2$
9	9	2^2	9	1	$3 \times Z^2$	1	9	2^8	9	1	$3 \times Z^2$	1	9	2^2	9	1	Z^8	1	9
10	10	3	20	Z^4	30	7	40	9	$2 \times Z^8$	11	60	13	70	$3 \times Z^4$	80	17	90	19	$4 \times Z^8$
11	11	1	11	1	11	1	11	1	11	2^{10}	11	1	11	1	11	1	11	1	11
12	12	Z^2	$6 \times Z^2$	5	$4 \times Z^4$	7	$12 \times Z^2$	$3 \times Z^2$	60	11	$2 \times Z^{10}$	13	84	$5 \times Z^2$	$24 \times Z^2$	17	$12 \times Z^4$	19	$30 \times Z^2$
13	13	1	13	1	13	1	13	1	13	1	2^{12}	13	1	13	1	13	1	13	
14	14	3	28	5	42	Z^6	56	9	70	11	84	13	$2 \times Z^{12}$	15	112	17	126	19	140
15	15	2^2	15	2^4	$5 \times Z^2$	1	15	2^2	$3 \times Z^4$	1	$5 \times Z^2$	1	15	2^{14}	15	1	$5 \times Z^2$	1	$3 \times Z^4$
16	16	3	$8 \times Z^2$	5	48	7	$4 \times Z^6$	9	80	11	$24 \times Z^2$	13	112	15	$2 \times Z^{14}$	17	144	19	$40 \times Z^2$
17	17	1	17	2	17	1	17	1	17	1	17	1	17	2^{16}	17	1	17	1	17
18	18	Z^2	36	5	$6 \times Z^4$	7	72	Z^8	90	11	$12 \times Z^4$	13	126	$5 \times Z^4$	144	17	$2 \times Z^{16}$	19	180
19	19	1	19	1	19	1	19	1	19	1	19	1	19	1	19	1	2^{18}	19	19
20	20	3	$10 \times Z^2$	Z^4	60	7	$20 \times Z^2$	9	$4 \times Z^8$	11	$30 \times Z^2$	13	140	$3 \times Z^4$	$40 \times Z^2$	17	180	19	$2 \times Z^{18}$

Table 2.1: $H_1(\Sigma(L))$ for (p, q) torus links with $2 \leq (p, q) \leq 20$. x implies a group \mathbb{Z}_x , integer summands are given as usual.

Figure 1.11: A ‘periodic table’ of homotopy classes of possible nematic textures for (p, q) torus links. Note the diversity: the sets may be finite or infinite, and where finite their size can vary dramatically.

One solution is a construction which generalises the dark brushes of Schlieren textures to three dimensions — the Pontryagin-Thom construction [Chen, 2012; Gupta and A. Saxena, 2018; Machon, 2016; Chen et al., 2013]. The idea is to extract the set of all points in the sample where the director is horizontal (more generally, perpendicular to some fixed direction in $\mathbb{R}P^2$). This is exactly what a Schlieren textures shows, although Schlieren textures contain some redundancy, showing us the set where the director is both horizontal and vertical — we only really need half this data. In a three dimensional sample this ‘horizontal set’ is not comprised of lines as in the two-dimensional Schlieren texture but is a surface,

the Pontryagin-Thom (PT) surface. After finding this surface, the construction is completed by colouring it according to the orientation in the horizontal plane that the director takes. An illustration of this procedure is shown in figure 1.12(a). A powerful result in Algebraic Topology called the Pontryagin-Thom correspondance [Milnor, 1997; Hatcher, 2002] shows that these coloured surfaces, taken up to smooth deformations (more precisely framed cobordisms), are in one-to-one correspondance with homotopy classes of maps, and so textures may be visually distinguished by their differing PT surfaces. To illustrate this fact, in figure 1.12(b) we show the two distinct PT surfaces for the two nonhomotopic Hopf link textures [Machon, 2016] (that they are both a single colour is an indication that representatives from both homotopy classes with the director everywhere in the sample perpendicular to some axis can be chosen). Returning to figure 1.7(c), this construction provides the coloured surfaces shown; by examining the surface and the colour windings upon it, we may place the texture in one of the classes from eq. (1.5). PT surfaces represent an enormous compression of information into a visually immediate form, and their utility is far from limited to disclination lines; we shall use them in our own work in §§??.

Now that we have seen some of the theoretical developments in knotted liquid crystals — the homotopy classification, the Pontryagin-Thom construction — let us remark again on the similarities and differences to fluids. Topological invariants play a vital role in both, linking and self linking in fluids and homology groups of the link complement in liquid crystals. Indeed, the self linking of liquid crystal textures will give rise to inequivalent colour windings on their PT surface and differing elements of the homotopy classification. However in contrast to fluids, where knot reconnections have been experimentally tracked and studied, there has been almost no mention of dynamics and link reconnections. When this happens, the topology of the link complement changes, and point defects may even be nucleated, perhaps a daunting theoretical task given that existing theory primarily assumes the domain is fixed, and even then finds a richness of possibility. We shall not develop this line of questioning further here, but invite the reader to consult Refs. ? for theoretical developments in this direction. In summary, we simply remark that it is increasingly clear the world of knotted fields is far broader than fluids.

1.3.3 Beyond disclination lines

The above sections focused on the knotting and nontrivial topology of disclination lines — defects in the director \mathbf{n} itself. Given the experimental focus on systems of this kind, and their direct connection to the idea of a knotted field, this is natural.

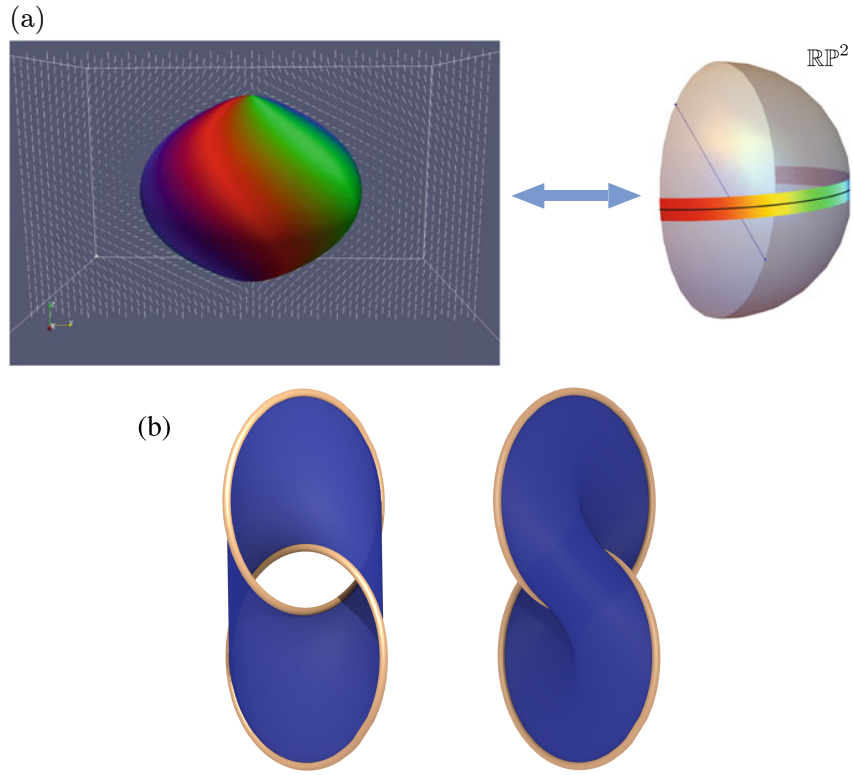


Figure 1.12: (a) The Pontryagin-Thom construction. The set where the director is horizontal, i.e. the preimage of the equator in \mathbb{RP}^2 , is extracted and coloured by its position on this equator (the angle the director makes in the horizontal plane). Note that in contrast to the more standard picture of \mathbb{RP}^2 shown in figure 1.9 here it is ‘turned on its side’ so that, visually, the horizontal plane through it (which one should imagine as also being the horizontal plane in the liquid crystal domain), does not coincide with the equator of the hemisphere. The texture shown here is a topologically nontrivial one called a toron [], containing two strength 1 point defects at its top and bottom, each detected by two rotations of the colour wheel on the PT surface. (b) Two distinct (noncobordant) PT surfaces for the Hopf link, representing the two possible nonhomotopic textures of figure 1.11. Figures reproduced from [Gupta and A. Saxena, 2018; Machon, 2016].

However even in the absence of defects liquid crystals support an array of topological phenomena which may also be considered examples of knotted fields, although perhaps in a different sense to those discussed above.

Skyrmions and Hopfions

The most well known topological feature of this kind is a skyrmion, an example of which is shown in figure 1.13 (a) given by the vector field $\mathbf{n}(r) = \cos(\pi r)\mathbf{e}_z + \sin(\pi r)\mathbf{e}_r$ on the unit disk. Fixing the director on the disk boundary, we may wrap this texture around a sphere (compactifying the boundary to a point) at which point its topology is captured by a map $\mathbf{n} : S^2 \rightarrow S^2$, in other words an element of $\pi_2(S^2) \approx \mathbb{Z}$. These textures are a well studied feature of vector and line fields in two dimensions [Gupta and A. Saxena, 2018]. We are primarily interested in the properties of order in three dimensions, and as such focus on their three dimensional ‘cousins’: Hopfions. An experimental image of a Hopfion is shown in figure 1.13(b)[Chen, 2012; Chen et al., 2013]. The figure shows a nematic liquid crystal texture inside a three dimensional cell, where the PT surface has been constructed by extracting director orientation via three-photon fluorescence microscopy. What qualifies the Hopfion as a knotted field becomes clear on viewing this surface: each stripe of colour twists about a torus, linking each other colour exactly once — in a Hopf link, no less. Skyrmions are classified by an element of $\pi_2(S^2)$. Hopfions are instead classified by $\pi_3(S^2)$, the third homotopy group of the sphere. Heinz Hopf famously showed that $\pi_3(S^2) \approx \mathbb{Z}$, and in doing so constructed an explicit example of a nontrivial element of this group — the celebrated Hopf Fibration. For mathematical detail on the construction of the fibration we refer to the reader to Refs. [Gupta and A. Saxena, 2018; Bott and Tu, 1982], and for an excellent video of its structure we urge the reader to consult Ref. [Johnson, 2011]. Figure 1.13(b) shows an experimental image of this fibration; the energetics of the liquid system favour a fixed far field nematic direction, mimicking the skyrmion boundary conditions and allowing the domain to be compactified $\mathbb{R}^3 \rightarrow S^3$. The nematic texture then realises a map : $S^3 \rightarrow \mathbb{RP}^2$, and $\pi_3(\mathbb{RP}^2) \approx \pi_3(S^2) \approx \mathbb{Z}$. The fact that the order lies in \mathbb{RP}^2 not S^2 is reflected in that fact that there are two stripes of each colour on the experimental fibration [Chen et al., 2013; Ackerman and Smalyukh, 2017]; in figures 1.13(c,d) we show a hopfion in vector order, containing only single stripes, with two particular stripes picked out to make the linking clear.

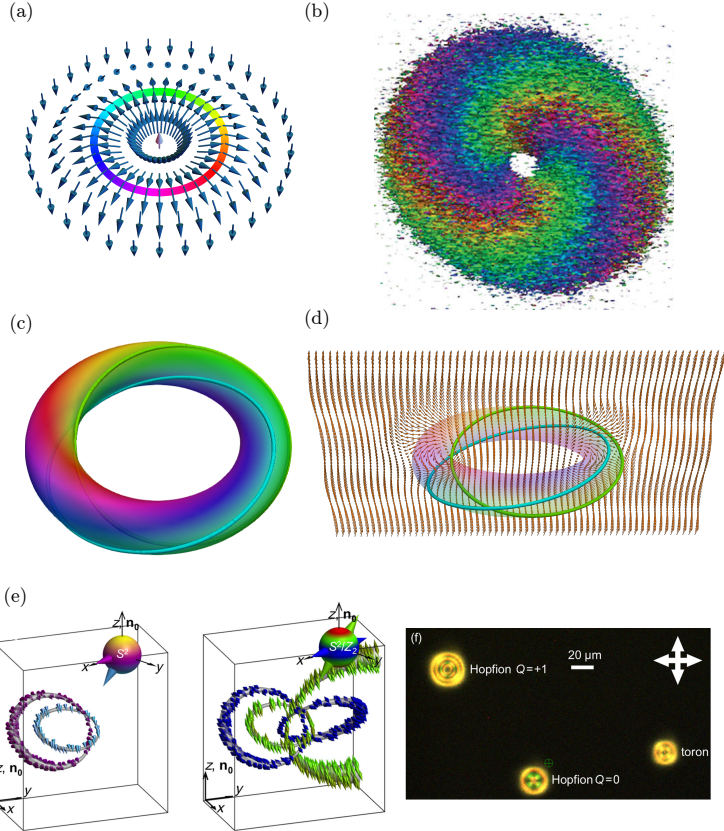


Figure 1.13: Defect free, topologically nontrivial textures. (a) A skyrmion given by $\mathbf{n}(r) = \cos(\pi r) \mathbf{e}_z + \sin(\pi r) \mathbf{e}_r$, classified by an element of $\pi_2(S^2) \approx \mathbb{Z}$, here +1. One way to visualise this is by plotting the PT surface for the skyrmion and noting its +1 winding. (b) An experimental image of a Hopfion in nematic order, with reconstructed PT surface. It is classified by an element of $\pi_3(\mathbb{R}P^2) \approx \mathbb{Z}$, here +1, which may be computed via the linking number of the different stripes of color. That there are two stripes of each colour reflects that fact that the order space is $\mathbb{R}P^2$ not S^2 (see the following figure). (c,d) A simulation of of Hopfion in vector order (order space S^2), with stripes of two colours picked out to aid visualisation of their linking. Note that in vector order there is only a single stripe of each colour. (d) shows a cross section of the director field corresponding to this Hopfion. (e) Recent experimental image of a Hopfion, clearly showing the telltale linking of preimages. The first panel shows a vectorized director, i.e. a choice of arrowhead has been made. In the second panel, it has not, and linking of two colours for antipodal vectors becomes linking of the same colour. (f) Polarizing optical micrograph of Hopfions and other textures. Arrows showed crossed polarizer directions, and the green circled cross denotes the size of the lazer tweezer which manipulates them. Figures (b,e,f) reproduced from [Chen et al., 2013; Ackerman and Smalyukh, 2017].

The geometry of vector fields

The linking of inverse images is the hallmark of the hopf texture (figure 1.13(e)). However without data processing, this linking is not an immeadiately apparent feature of the director. By contrast the knotted disclinations, and even their associated PT surface, in figure 1.7 may be clearly visualised. This is a consequence of the coupling of these topological features to the geometry, energetics and ultimately interaction with light of the liquid crystal, a coupling not present in the inverse images charecterising the Hopfion in figure 1.13 (e). This observation invites the question: are there ‘natural’ features of the Hopfion, or nonsingular liquid crystal textures in general, which can be used to infer their topology? We will explore this question, with a particular focus on a recent discovered phase of liquid crystal, in §§???. The focus will be on naturally geometric structures inside the liquid crystal which also contain some topological information, and so we now discuss the geometry of liquid crystals, and vector fields more generally.

The fundamental geometry and energetics of nematics was encoded by Frank in 1958 [Frank, 1958], where he gave a free energy for their elastic distortions. We give this free energy here in a slightly nonstandard form, following Ref. [Selinger, 2019]:

$$F = \int d^3\mathbf{r} \quad \frac{K_1}{2}(\nabla \cdot \mathbf{n})^2 + \frac{K_2}{2}(\mathbf{n} \cdot \nabla \times \mathbf{n})^2 + \frac{K_3}{2}(\mathbf{n} \cdot \nabla)\mathbf{n} + \frac{K_{24}}{2}\text{Tr}(\Delta)^2, \quad (1.6)$$

where the various K_i are elastic constants⁴. Each term in eq. 1.6 comes from a different mode of distortion for the liquid crystal, shown in figure (1.14):

$$(\mathbf{n} \cdot \nabla)\mathbf{n} \quad \text{Bend}, \quad (1.7)$$

$$\mathbf{n} \cdot \nabla \times \mathbf{n} \quad \text{Twist}, \quad (1.8)$$

$$\nabla \cdot \mathbf{n} \quad \text{Uniaxial Splay}, \quad (1.9)$$

$$\Delta(\bullet) := \frac{1}{2} \left((\bullet \cdot \nabla \mathbf{n}) + \mathbf{n} \times (\mathbf{n} \times \bullet \cdot \mathbf{n}) \right) \quad \text{Biaxial Splay}. \quad (1.10)$$

Vector order has a local rotational symmetry under which the free energy eq. (1.6) must remain invariant, and indeed the above terms are exactly those combinations of gradients which respect this symmetry. More precisely, the terms appearing in eq. (1.6) correspond to the magnitudes of the irreducible representations of $\nabla \mathbf{n}$ under the action of the rotation group $SO(2)$. These piece together to give a decomposition of $\nabla \mathbf{n}$ which is naturally written in terms of gradients parallel and perpendicular to

⁴These constants do not match one-to-one with those found in the standard writing of the Frank free energy; see Ref. [Selinger, 2019].

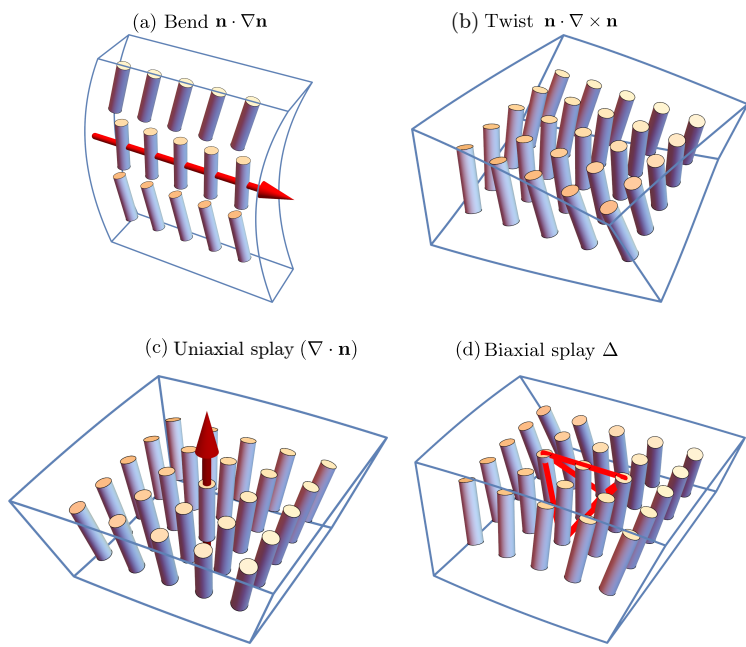


Figure 1.14: The four modes of director deformation: Bend, Twist, (uniaxial) splay and biaxial splay. The vector plotted in (c) is the splay vector $(\nabla \cdot \mathbf{n})\mathbf{n}$. Biaxial deformations, described by a rank two tensor (not a vector as in (a),(c)) are represented by a tetrahedron corresponding to the triple $\{\mathbf{n}, \Delta_1, \Delta_2\}$, where Δ_i denotes the i th eigenvector of Δ . Figures reproduced from [Selinger, 2019].

the director, $\nabla \mathbf{n} = \nabla \mathbf{n}_{\parallel} + \nabla \mathbf{n}_{\perp}$, where

$$\nabla \mathbf{n}_{\parallel} = \mathbf{n}^* \otimes (\mathbf{n} \cdot \nabla) \mathbf{n} \quad (1.11)$$

$$\nabla \mathbf{n}_{\perp} = \frac{\nabla \cdot \mathbf{n}}{2} I - \frac{\mathbf{n} \cdot \nabla \times \mathbf{n}}{2} J + \Delta. \quad (1.12)$$

I is the identity transformation, and $J = \mathbf{n} \times \bullet$ is rotation about \mathbf{n} .⁵ The geometry of $\nabla \mathbf{n}_{\perp}$ and Δ in particular has been explored in Ref. [Machon and Alexander, 2016b]. $\nabla \mathbf{n}_{\perp}$ describes how \mathbf{n} varies as one moves in a plane perpendicular to it; this is a classical object in differential geometry of surfaces called the shape operator. The decomposition eq. 1.12 corresponds to its breakdown into an isotropic piece I , an antisymmetric piece J and a traceless symmetric piece Δ (if \mathbf{n} were the normal to a family of surfaces the antisymmetric piece would vanish). All directional information is contained in Δ ; its eigenvectors coincide with those of $\nabla_{\perp} \mathbf{n}$ and pick out the two directions of principal curvature in plane perpendicular the director. This explains the name ‘biaxial splay’ for its mode of distortion. The geometry of $\nabla \mathbf{n}_{\parallel}$ is less well explored. It describes the bending of the director field: if one traces a single curve to which \mathbf{n} is tangent, then $\nabla \mathbf{n}_{\parallel}$ gives the classical curvature from the differential geometry of space curves [DoCarmo, 1976]. A more complete account of its geometry will in part be the topic §§??.

Each of the pieces in eq. 1.12 is manifestly geometric, but they also represent topological information, as canonical sections of vector bundles defined by the director. At each point in the material, the director \mathbf{n} splits the tangent space into a line parallel to \mathbf{n} , L_n , and a plane perpendicular to it, ξ , $T\mathbb{R}^3 \approx L_n \oplus \xi$. An example of this splitting for a skyrmion texture is shown in figure 1.15. The families of lines L_n and planes ξ vary smoothly with the director, and such smoothly varying families of vector spaces are called vector bundles [Tu, 2010; Milnor and Stasheff, 1974]. The most famous example of a vector bundle, and the interesting properties they can have, is the family of planes tangent to S^2 (its tangent bundle). The Poincare-Hopf theorem tells us one cannot ‘comb a sphere’ [Milnor, 1997], in other words one cannot choose a nonzero tangent vector everywhere on the sphere. Said more technically, one cannot find an everywhere nonzero section of the tangent bundle to the sphere. This failure is connected to the topology of S^2 ; if one sums the windings of all the zeros in the vector field one obtains the Euler Characteristic of S^2 . An entirely analogous result holds for any vector bundle; the zeros of a section of a vector bundle encode its Euler Class [Bott and Tu, 1982; Milnor and Stasheff,

⁵That the twist and splay terms appear squared in eq. 1.6 is because the decomposition eq. 1.12 is for vector order, not nematic order. The additional symmetry $\mathbf{n} \sim -\mathbf{n}$ forces us to square these terms.

1974]. Returning to eq. 1.12, $\nabla_{\perp} \mathbf{n}$ is a section of the bundle $\xi^* \otimes \xi$ — it maps vectors orthogonal to \mathbf{n} into vectors orthogonal to \mathbf{n} — and the bend $\nabla_{\parallel} \mathbf{n}$ is a section of the bundle $L_n^* \otimes \xi$. Both probe the topology of ξ and, loosely speaking, as ξ is in one-to-one correspondance with the director \mathbf{n} this topology carries over to \mathbf{n} . The zeros of Δ , called umbilic lines in analogy to the umbilic points of the differential geometry of surfaces, have been investigated in Ref. [Machon and Alexander, 2016b]. The zeros of $\nabla_{\parallel} \mathbf{n}$, which we will call β lines, will be the subject of §§??.

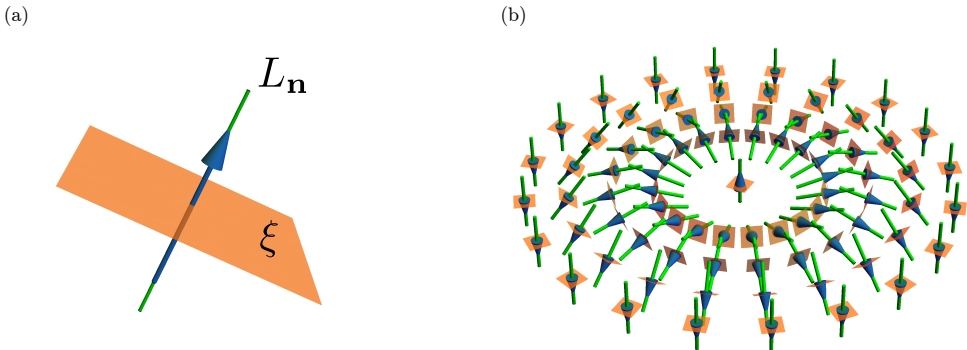


Figure 1.15: The director \mathbf{n} splits space into families of lines L_n parallel to it, and a family of planes ξ perpendicular to it: $T\mathbb{R}^3 \approx L_n \oplus \xi$. Panel (a) shows this splitting at one point, with the director a blue arrow, L_n the green line and ξ the orange plane. This splitting is shown for an entire skyrmion texture in panel (b). A smoothly varying choice of vectors tangent to the family of planes ξ (section of the bundle) cannot be made here, reflecting the fact the skyrmion texture is topologically the family of normal vectors to S^2 , and ξ is its tangent bundle.

The umbilic and β lines are natural geometric structures found in any vector field. However, they assume a particular relevance when strongly coupled to the energetics of the liquid crystal texture. One way to do this is to frustrate the liquid crystal with boundary conditions, as in the disclinations of figure 1.7. Another is to pass to a different phase of liquid crystal, where such coupling exists. In the case of umbilic lines, this setting is the cholesteric phase [Beller et al., 2014], in which the liquid crystal has a preference for nonzero twist; Δ turns out to be related to the axis of this twisting [Gupta and A. Saxena, 2018], and its zeros thus encode energetic frustration inside the cholesteric [Machon and Alexander, 2016b]. For β lines, the natural setting is a recently discovered phase of liquid crystal, the twist-bend or splay-bend nematic [Jákli et al., 2018]. These materials, comprised of banana shaped molecules, have an energetic preference for everywhere nonzero bend.

A second focus of §§?? will be on this interplay between geometry and energetics in twist-bend nematics.

1.4 Modern knotted fields: Excitable Media

“In excitable media we may have a new context in which something like a vortex atom theory can live again, strangely transfigured.”

A. T. Winfree, The Geometry of Biological Time, Chapter 9.

We now come to our final example of knotted fields, those found in excitable media. We might have discussed them immediately after fluids and superfluids, and indeed we will see closer similarities to those systems than to liquid crystals. That we choose not to is a reflection of their relative lack of experimental development. By way of prelude, the modern state of affairs in these systems is that the analogy to a fluid vortex ring can be generated experimentally. Figure 1.16(a) shows a schematic of a thick dish of the Belousov-Zhabotinsky (BZ) reagent, a medium which support waves of propagating chemical activity. Axially symmetric waves of such activity spiral outwards from a ‘singular’ ring shown in red — exactly what is occurring on this ring will be discussed below. Figure 1.16(b) shows an experimental realisation of this setup from [Totz et al., 2015], viewed from the side in figures (a)–(e) and from the top in (f)–(g). From the side the ring appears as a discontinuity in the emitted wavefronts, with a second such discontinuity where the fronts collide in the middle of the dish. The overlaid red curves track the position of this ring. They show, firstly, that it stably persists over several hours, and secondly that it has its own dynamics, expanding, contracting or reaching a stable radius (the outcome may be experimentally tuned). The topological possibilities, dynamics, and organisation of the entire excitable medium by these rings are the subject of this section, and of §§??. These rings have not been experimentally tied in nontrivial configurations, but proposals exist ?. As we shall see in this section, such an experiment would be extremely interesting.

Excitable media

The building block of an excitable medium is an excitable oscillator, something which rests in a quiescent locally stable state but which, given a small kick, becomes excited before relaxing back to quiescence. A prototypical example is a nerve cell. Given an electrical input, the cell ‘fires’, becoming excited, before slowly relaxing back to its resting state where it can be triggered again. An excitable medium is

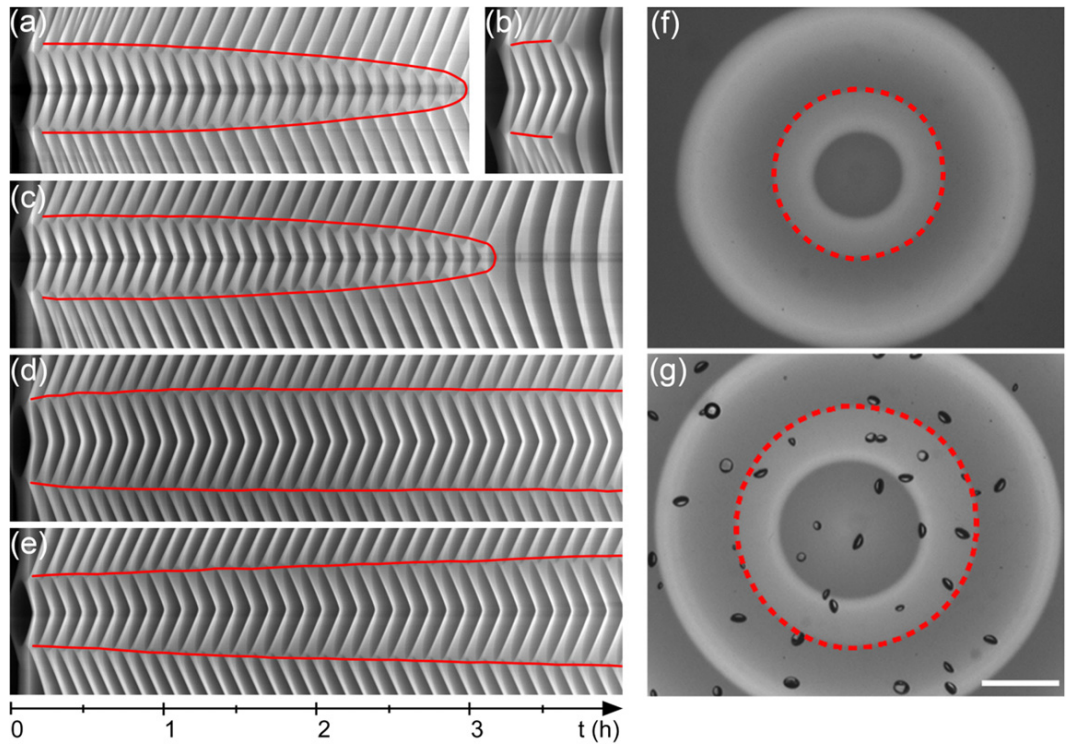
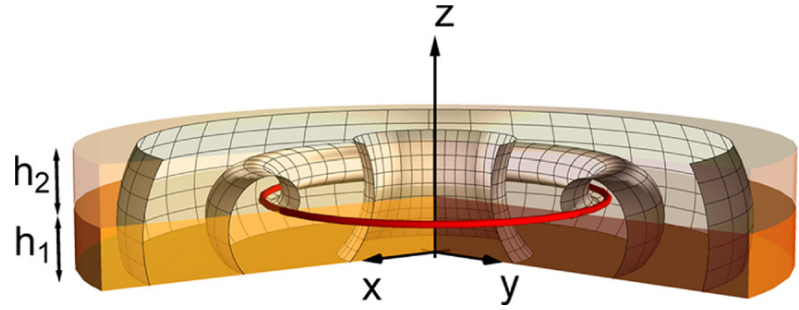


Figure 1.16: Top Panel: Schematic illustration of a vortex ring in excitable media. A dish of the Belusov-Zhabotinsky reagent supports an axially symmetric spiralling wave of chemical activity (meshed wavefronts) emanating from a ring shaped singularity shown in red. Bottom Panel: An experiment realising this setup. (a)-(e) shows a time series of the dish viewed side on, i.e the x - z plane, over 4 hours. The rotation period of the wave itself is $390\text{s} \approx 6\text{-}7\text{ mins}$. In each frame, the ring appears as a pair of points with wavefronts emanating from it, which collide in the middle of the dish. Over time the ring moves, tracing the curves shown. Depending on the heights h_1 and h_2 it may shrink (a),(c), reach a steady radius (d) or expand (e). (f) and (g) show the ring from above (x - y plane) over 3 hours. Setting spatial scale, the white bar in (g) corresponds to 5 mm. Figures reproduced from [Totz et al., 2015].

a continuum of these oscillators, all coupled together, in our case by diffusion of activity from one oscillator to its spatial neighbours. Such media support waves of activity, where an excitation in one oscillator triggers its neighbours to ‘fire’ also. A pleasing example of such waves is a grass fire Winfree and Strogatz [1983a]. The oscillators are blades of grass. Their resting state is unburnt, their excited state burnt. After burning, the blades slowly grow back, able to be burnt again. A field of grass, the excitable medium, supports a wave of excitation, i.e. a moving front of grass fire. Note the front has a leading edge (the transition from unexcited to excited) and a trailing edge (the transition from excited to unexcited).

There is an enormous experimental and theoretical literature on systems exhibiting this sort of behaviour; for references see [Winfree, 2001]. We present a minimal mathematical model, which shall be the focus of §§??, and which provides an effective description of many more complex excitable media [Winfree, 2001]: the Fitzhugh-Nagumo model [FitzHugh, 1961; Nagumo et al., 1962]

$$\frac{\partial u}{\partial t} = \frac{1}{\epsilon}(u - \frac{1}{3}u^3 - v) + \nabla^2 u, \quad (1.13)$$

$$\frac{\partial v}{\partial t} = \epsilon(u + \beta - \gamma v). \quad (1.14)$$

Here $u(\mathbf{x}, t)$, $v(\mathbf{x}, t)$ are two real valued scalar fields, with ϵ, γ, β model parameters. The coupling which turns this system from an excitable oscillator to an excitable medium is through diffusion $\nabla^2 u$, in this instance in the u variable only (although variants with diffusion in each variable also exist). The phase plane for the ODE system without diffusion is shown in figure 1.17(a), with parameter choices which will generate an excitable oscillator. The system has a fixed point (u^*, v^*) (black dot), but given a finite perturbation in u it will execute a large loop in phase space, jumping to the upper branch of the u nullcline, crawling along it until the first inflection, whereupon it jumps to the lower branch and crawls again back to the fixed point (black arrows in the figure). In the sense that a perturbation in u instigates this loop, u might be considered an ‘excitor’ variable and v a ‘recovery’ variable.

The topological possibilities of excitable media

The key topological observation is that the excitation-recovery loop is a circle S^1 . In a portion of excitable media M , the state of a typical point lies somewhere on this loop, and thus we can describe the system with a map $\phi : M \rightarrow S^1$, a situation encountered before in superfluids. Concretely mapping between (u, v) and ϕ may be achieved via something of the form $(u, v) = (2 \cos \phi - u^*, \sin \phi - v^*)$, stretching S^1

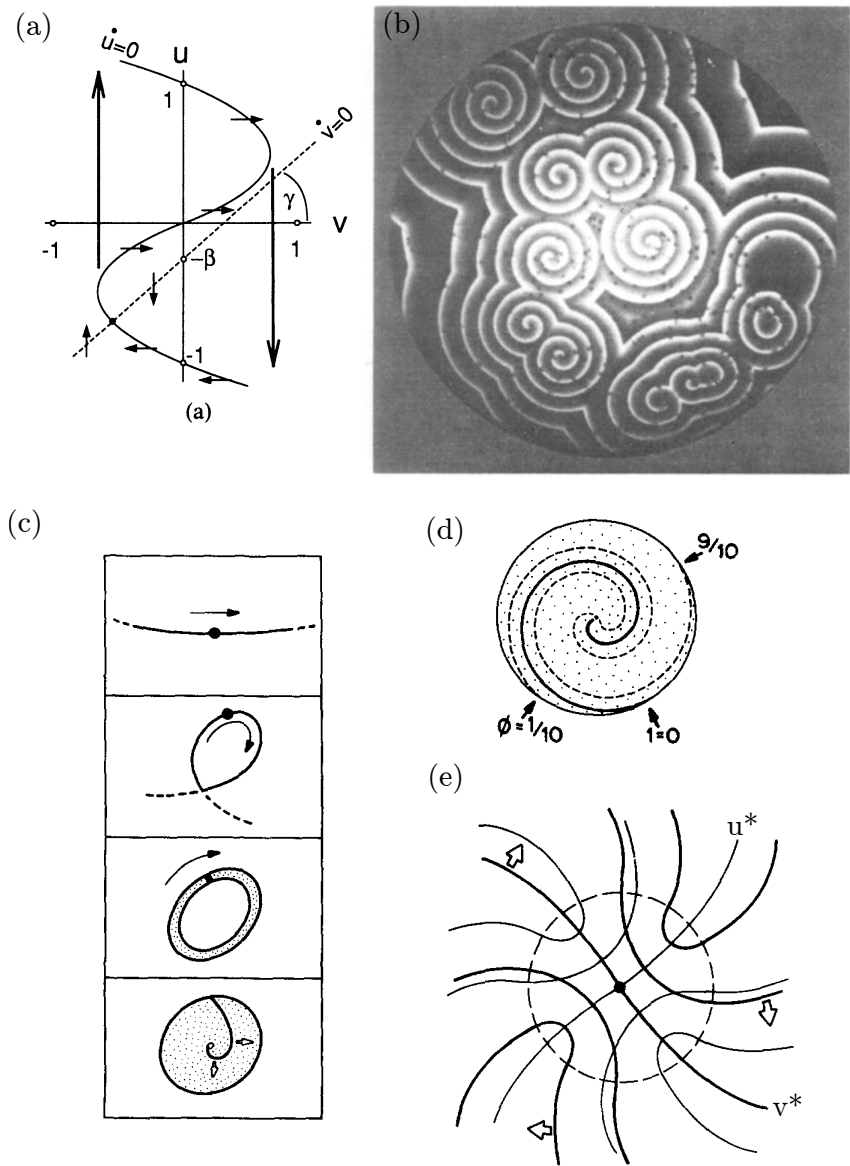


Figure 1.17: Spiral waves in two dimensions. (a) The phase plane of the FitzHugh-Nagumo model eq. 1.14, with u and v nullclines (solid and dotted curves), fixed point (black dot) and excitation-recovery loop (large black arrows) shown. This loop is topologically a circle S^1 , and progression through a cycle of excitation-recovery can be described by a phase $\phi \in S^1$. (b) Spiral waves in a dish of the BZ reagent. (c) –(e) The anatomy of a single spiral wave. In (c) one imagines setting a pulse of excitation running around a closed loop, which gradually thickens until the propagation time around its inner edge is faster than the medium can recover. The resulting structure is a spiral wave. (d) shows its phase description, with three example isophase spirals are shown. (e) A qualitative picture of the (u, v) field around a spiral wave vortex. Away from the vortex the contours are parallel, but inside they necessarily cross one another transversally. Figures reproduced from [Winfree and Strogatz, 1983a].

over the excitation-recovery loop. That the system is characterised by the phase field $\phi \in S^1$ immediately implies the potential existence of knotted and linked vortices if our domain M is three-dimensional, again by simple analogy with superfluids. What makes this system so interesting is that the character and dynamics of these phase singularities are very different to what we have encountered before.

In two dimensions these singularities are at the core of spiral waves, a collection of which are shown in the BZ reagent in figure 1.17(b). The anatomy of a single spiral wave is dissected in figure 1.17(c)–(e). In figure 1.17(c), one imagines taking an initially thin ring of excitable medium and setting a wave of excitation running around it. If the ring is thickened, we expect some spatial variation in the wavefront—it turns out that given isotropic diffusion in eq. 1.14 it takes the shape of an involute spiral started from the inner edge of the annulus [Winfree, 2001]. This thickening process happily continues until the time taken for the inner edge of the wave to circulate once is comparable to the recovery time of the medium, a condition which defines a ‘core region’, inside of which the (u, v) states of points leave the excitation-recovery loop and so cannot be reliably assigned a phase ϕ (this is analogous to what happens inside the healing lengthscale which sets vortex core size in superfluids). A phase description in which the core is idealised to zero radius is shown in figure 1.17(d), and a qualitative picture of the corresponding contours of (u, v) is shown in figure 1.17(e). These ‘rotors’ periodically emanate waves of excitation which organise the entire medium, splitting it into domains separated by shock structures where two wavefronts coincide and annihilate (figure 1.17(b)).

TODO: SOMETHING ABOUT LENGTH AND TIMESCALES

In three dimensions, we have a linelike phase singularity, a vortex filament, emitting ‘scroll waves’. The geometric and topological possibilities of linked and knotted vortex filaments were first investigated in a series of papers by A.T. Winfree and S. Strogatz [Winfree and Strogatz, 1983a,b,c, 1984]. The simplest possibility is for filament to close into a ring, emitting axially symmetric waves which fill space as shown in figure 1.18 (a). This is the scenario was encountered experimentally in figure 1.16. However, Winfree and Strogatz demonstrated numerous other possibilities. For example, we once again have internal structure along the singularity, in this case the phase of rotor in successive cross sections along the filament, which opens up the possibility of self linking. The simplest such scenario, a twisted scroll wave, is shown in figures (b) and (c). Focusing on figure (c), we note that such twisting implies a full cycle of phase about a line threading the hole in the ring. In other words, a second phase singularity must exist along this line too! Closing this line into a second loop, we obtain figure (d); two scroll rings, each with linking and

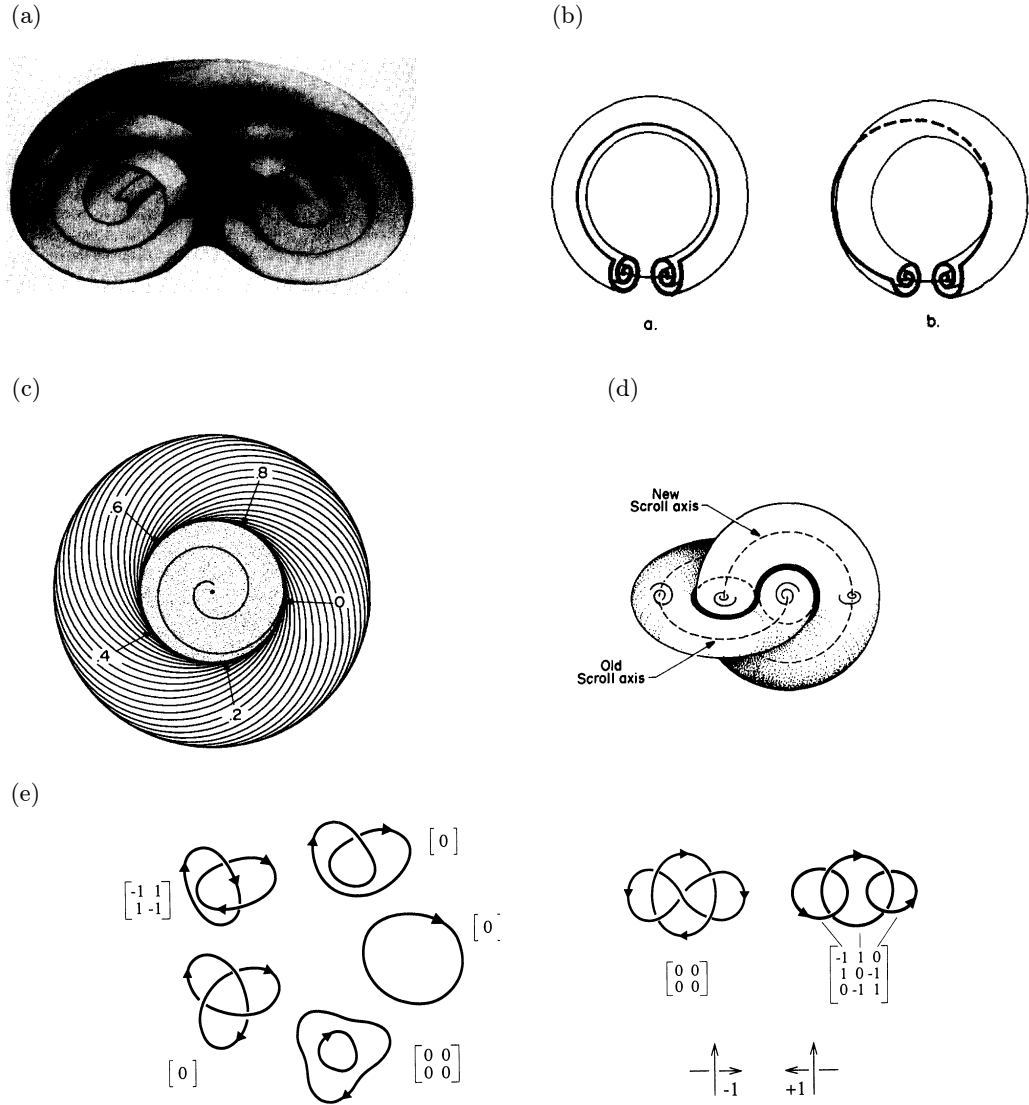


Figure 1.18: the topological possibilities of knotted vortices in excitable media. (a) A spiral wave rotated around an axis of symmetry forms a scroll wave, shown in cross section with wavefronts in grey. This is the system realised in figure 1.16. (b) Cutting a scroll wave, putting a full turn of twisting into it, then gluing back together. (c), (d): This twisted scroll ring has a full cycle of phase around its equator (points 0 through 8 in (c)), necessitating the existence of a second twisted scroll ring linking the first, shown in (d). (e) Two groups of knotted vortices, with transmutations topologically allowed between neighboring elements of each group. The matrices shown have i, j th element $LK(C_i, C_j)$, where $LK(C_i, C_i) := SL(C_i)$. Note each row (and column) sums to zero, an expression of eq. 1.15. Figures reproduced from [Winfree and Strogatz, 1983a,b; Winfree, 1990].

self linking number (+)1. Winfree and Strogatz extend this line of reasoning in a manner familiar to that of Moffatt [Moffatt, 1969] to derive a topological selection rule on allowed configurations of knotted vortices:

$$0 = \sum_{i,j,i \neq j} Lk(C_i, C_j) + SL(C_i) \quad \forall i. \quad (1.15)$$

This rule has a similar feel to the helicity count of eq. (1.3), but its content is slightly different. It is a condition each knotted loop in a link must satisfy in order for the whole to exist. We note briefly that one might be tempted to use eq. (1.15) as a basis for a definition of Helicity in excitable media. In fact a continuum definition of a helicity has been given [Trueba and Arrayás, 2009] but it is currently not clear (to me at least) how the concepts interlink; it is an interesting question for further study.

The dynamical possibilities of excitable media

Provided the topological constraint eq. (1.15) remains satisfied, there is no reason link reconnections cannot occur, as they do in the other systems we have discussed. In figure 1.18(e) we show two groups of allowed knotted vortices, and within each group transmutations are topologically allowed. As Winfree and Strogatz note, questions of whether or not they actually occur in a given excitable medium “probably depend sensitively on the exact kinetics of the medium” [Winfree and Strogatz, 1984]. For example, in the experiment of 1.16(b) [Totz et al., 2015] we saw that these vortex lines are not merely static emitters of wavefronts, they have their own dynamics, and one has no *a priori* reason to expect these dynamics to preserve topology. What is absolutely remarkable is that, in a certain parameter regime in the FitzHugh-Nagumo model, it was found that they do [Winfree, 1990; Henze, 1993]. Using $\epsilon = 0.3, \beta = 0.7, \gamma = 0.5$, a stable vortex ring was found in [Courtemanche et al., 1990], shown in figure 1.19(a), followed by a stable trefoil knot [Henze and Winfree, 1991](in a slightly different kinetics) and then a variety of apparently stable knots and links [Henze, 1993] summarised in figure 1.19(b). An account of this first period of development may be found in Refs. [Winfree, 1990, 2001; S. J. Hogan, 2002]. Subsequent work [Sutcliffe and Winfree, 2003] confirmed a wide basin of stability for the trefoil knot and the Hopf link over substantially larger time periods than the original trefoil simulations were run for. More recently, Maucher and Sutcliffe [Maucher and Sutcliffe, 2016] showed that the FitzHugh-Nagumo dynamics is even capable of simplifying a tangled unknot into a unique canonical round form and demonstrated stable forms for more complex knots — the figure-eight and torus

links in certain geometries [Maucher and Sutcliffe, 2017]. A simplification of a 13 crossing knot is shown in figures 1.19(c), with a cross section to show the associated wavefield in figure 1.19 (d) (one might compare to figure 1.17(b)). The stable torus and figure-eight knots with associated minimal lengths are shown in figure 1.19(e). These numerical findings are in stark contrast to what we saw in fluids, superfluids and liquid crystals (indeed, in most knotted fields), and invite a series of questions: What determines the dynamics of these vortices? How are reconnections avoided? What is the mechanism of knot untangling? Are all knots stable, and if so can we predict their shapes? In some form these questions have existed since the first knotted vortices were discovered. Initial theoretical work focused heavily on the idea that their laws of motion could be explained by a ‘local geometry hypothesis’ [Keener, 1988; Keener and Tyson, 1992; Henry and Hakim, 2002; Biktashev et al., 1994; Echebarria et al., 2006; Dierckx, 2010] in which dynamics at each point on the curve were governed by some local law of motion involving its curvature, the twist of spiral wave phase etc. After a perturbative theory for such a law was developed [Keener, 1988; Keener and Tyson, 1992; Biktashev et al., 1994], substantial work went into testing whether or not this was the case [Henze, 1993; Winfree, 1990], of which an account may be found in [S. J. Hogan, 2002]. Summarising very coarsely, such laws found some success in describing isolated filaments, but of course encounter problems whenever interfilament interactions are required. The problem is that evidence ultimately suggested such interactions were integral to describing stable knots [Henze, 1993; S. J. Hogan, 2002], and as such a local geometry hypothesis failed to account for their dynamics. The observed untangling without reconnection of unknots shown in figure 1.19(e) [Maucher and Sutcliffe, 2016] further casts doubt on whether such a law could be made to work.

We remark that the idea of reducing the dynamics of an entire field to that of a curve is not unique to excitable media, but cuts across knotted fields. In particular the idea is similar to the Local Induction Approximation (LIA) in fluids and superfluids [Saffman, 1992], in which the Biot-Savart law of motion governing vortex lines is approximated by a dominant contribution arising from local curvature, which leads to motion binormal to the curve — in the case of a vortex ring, drift perpendicular to the plane it lies in, a feature shared by the rings studied here [Winfree, 1990]. Further, exact knotted solutions to the LIA *do* exist [Kida, 1981; Hasimoto, 1972], and one might have hoped something similar applied here. Note however that the LIA breaks down in fluids too, and further that the nature of the fields surrounding the vortices is quite different between the two cases. One crucial difference, as we shall see, is that in excitable media waves propagate without

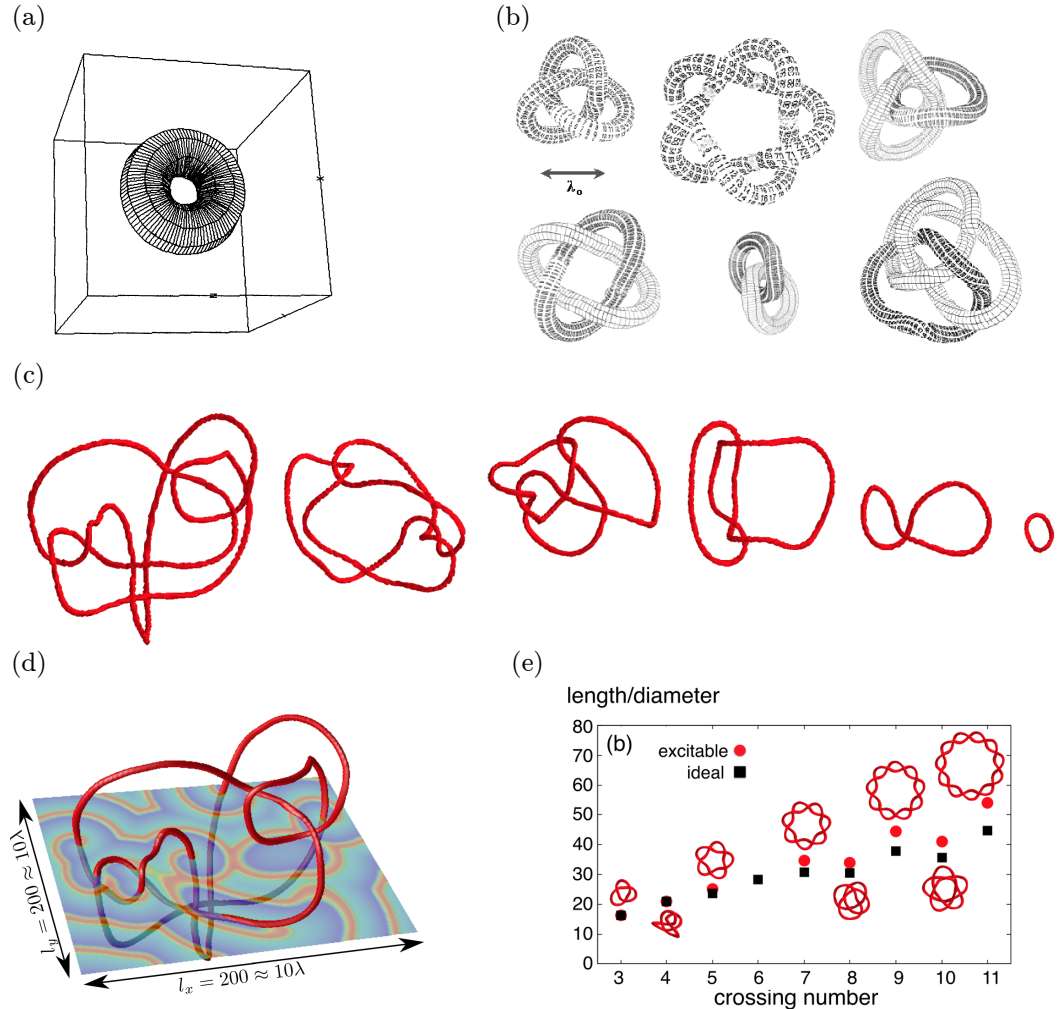


Figure 1.19: Stable knotted vortices in the FitzHugh-Nagumo model. (a) A vortex ring contracts to a stable radius and drifts at constant velocity; its radius is $0.23\lambda_0$, where λ_0 is the wavelength of the spiral wave in the medium (see scale bar in (b)). (b) An assortment of apparently stable knotted and linked vortices found in [Henze, 1993]. The tube around the knots is of diameter λ_0/π . The stability of the trefoil knot and Hopf link were subsequently confirmed in Ref. Sutcliffe and Winfree [2003] (the others are, in fact, unstable). (c,d) The FitzHugh-Nagumo dynamics are capable of simplifying a tangled, but unknotted, curve to the canonical round form of panel (a); panel (c) shows an example simplification, with a cross section through the vortex knot in (d) showing the wavefield. (e) Recently, stable forms for torus knots and the figure-eight knot were found. Their geometries are shown here, alongside their lengths as compared to ideal ropelengths. Figures reproduced from [Winfree, 1990; S. J. Hogan, 2002; Maucher and Sutcliffe, 2016, 2017].

attenuation for potentially arbitrary distances, making a theoretical decoupling of distant segments of the knot difficult.

In summary, the questions posed above are not satisfactorily answered. Our attempts to explore them, with a focus on systematically testing knots for stability and exploring the importance of nonlocal filament interactions, form §§???. The potential for experimentally accessible, and spontaneously stable, knotted fields is a major motivator for this work.

1.5 Structure of this Thesis

Bibliography

- Paul J. Ackerman and Ivan I. Smalyukh. Diversity of knot solitons in liquid crystals manifested by linking of preimages in torons and hopfions. *Phys. Rev. X*, 7:011006, Jan 2017. doi: 10.1103/PhysRevX.7.011006. URL <https://link.aps.org/doi/10.1103/PhysRevX.7.011006>.
- G. P. Alexander, B. G. Chen, E. A. Matsumoto, and R. D. Kamien. Colloquium: Disclination loops, point defects, and all that in nematic liquid crystals. *Rev. Mod. Phys.*, 84:497–514, 2012.
- Daniel A. Beller, Thomas Machon, Simon Čopar, Daniel M. Sussman, Gareth P. Alexander, Randall D. Kamien, and Ricardo A. Mosna. Geometry of the cholesteric phase. *Phys. Rev. X*, 4:031050, Sep 2014. doi: 10.1103/PhysRevX.4.031050. URL <https://link.aps.org/doi/10.1103/PhysRevX.4.031050>.
- V. N. Biktashev, A. V. Holden, and H. Zhang. Tension of organizing filaments of scroll waves. *Phil. Trans. R. Soc. A*, 347:611, 1994.
- R. Bott and L. Tu. *Differential forms in algebraic topology*. Springer-Verlag, 1982.
- B. G. Chen. *Topological defects in nematic and smectic liquid crystals*. PhD thesis, University of Pennsylvania, 2012.
- B. G. Chen, P. J. Ackerman, G. P. Alexander, R. D. Kamien, and I. I. Smalyukh. Generating the hopf fibration experimentally in nematic liquid crystals. *Phys. Rev. Lett.*, 110:237801, 2013.
- M. Courtemanche, W. Skaggs, and A.T. Winfree. Stable three-dimensional action potential circulation in the fitzhugh-nagumo model. *Physica D*, 41:173, 1990.
- G. Călugăreanu. L'intégrale de gauss et l'analyse des noeuds tridimensionnels. *Rev. Math. Pures Appl.*, 4:5–20, 1959.

- G. Călugăreanu. Sur les classes d'isotopie des noeuds tridimensionnels et leurs invariants. *Czechoslovak Math. J.*, 11:588–625, 1961.
- M. R. Dennis and J. H. Hannay. Geometry of călugăreanu's theorem. *Proc. R. Soc. A*, 461:3245–3254, 2005.
- M. R. Dennis, R. P. King, B. Jack, K. O'Holleran, and M. J. Padgett. Isolated optical vortex knots. *Nat. Phys.*, 6:118–121, 2010.
- H. Dierckx. *Dynamics of wave fronts and filaments in anisotropic cardiac tissue*. PhD thesis, The University of Ghent, 2010.
- M. DoCarmo. *Differential geometry of curves and surfaces*. Pearson, 1976.
- B. Echebarria, V. Hakim, and H. Henry. Nonequilibrium ribbon model of twisted scroll waves. *Phys. Rev. Lett.*, 96:098301, 2006.
- R. FitzHugh. Impulses and physiological states in theoretical models of nerve. *Bioophys. J.*, 1:445–466, 1961.
- F. C. Frank. I. liquid crystals. on the theory of liquid crystals. *Discuss. Faraday Soc.*, 25:19–28, 1958. doi: 10.1039/DF9582500019. URL <http://dx.doi.org/10.1039/DF9582500019>.
- S. Gupta and editors. A. Saxena. *The Role of Topology in Materials*. Springer International Publishing, 2018.
- H Hasimoto. A soliton on a vortex filament. *Journal of Fluid Mechanics*, 51:477485, 1972.
- A. Hatcher. *Algebraic Topology*. Cambridge: Cambridge University Press, 2002.
- H. Helmholtz. Über integrale der hydrodynamischen gleichungen, welche den wirbelbewegungen entsprechen. *J. fur die reine und angew Math*, 55:25–55, 1858.
- H. Henry and V. Hakim. Scroll waves in isotropic excitable media: Linear instabilities, bifurcations and restabilized states. *Phys. Rev. E*, 65:046235, 2002.
- C. Henze. *Vortex filaments in three dimensional excitable media*. PhD thesis, The University of Arizona, 1993.
- C. Henze and A.T. Winfree. A stable knotted singularity in an excitable medium. *Int. J. of Bifurcation and Chaos*, 1:891, 1991.

- W.T.M. Irvine. Moreau’s hydrodynamics helicity and the life of vortex knots and links. *Comptes Rendus Mécanique*, 346:170–174, 2018.
- Antal Jákli, Oleg D. Lavrentovich, and Jonathan V. Selinger. Physics of liquid crystals of bent-shaped molecules. *Rev. Mod. Phys.*, 90: 045004, Nov 2018. doi: 10.1103/RevModPhys.90.045004. URL <https://link.aps.org/doi/10.1103/RevModPhys.90.045004>.
- N. Johnson. A visualization of the hopf fibration, 2011. <https://nilesjohnson.net/hopf.html>.
- J. P. Keener. The dynamics of three-dimensional scroll waves in excitable media. *Physica D*, 31:269, 1988.
- J. P. Keener and J. J. Tyson. The dynamics of scroll waves in excitable media. *SIAM Rev.*, 34:1, 1992.
- S Kida. A vortex filament moving without change of form. *Journal of Fluid Mechanics*, 112:397409, 1981.
- D. Kleckner and W.T.M. Irvine. Creation and dynamics of knotted vortices. *Nat. Phys.*, 9:253–258, 2013.
- S. Van Der Laan. The vortex theory of atoms. Master’s thesis, Utrecht University, 2012.
- W. B. R. Lickorish. *An Introduction to Knot Theory*. New York: Springer-Verlag, 1997.
- S. J. Lomanaco. The modern legacies of thomson’s atomic vortex theory in classical electrodynamics. *AMS Proc. Symp. Appl. MathM*, 51:145–166, 1996.
- T. Machon. *Aspects of geometry and topology in liquid crystalline phases*. PhD thesis, University of Warwick, 2016.
- T. Machon and G. P. Alexander. Knotted defects in nematic liquid crystals. *Phys. Rev. Lett.*, 113:027801, Jul 2014.
- T. Machon and G. P. Alexander. Global defect topology in nematic liquid crystals. *Proc. R. Soc. A*, 472, 2016a.
- T. Machon and G. P. Alexander. Umbilic lines in orientational order. *Phys. Rev. X*, 6:011033, 2016b.

- F. Maucher and P. Sutcliffe. Untangling knots via reaction-diffusion dynamics of vortex strings. *Phys. Rev. Lett.*, 116:178101, 2016.
- F. Maucher and P. Sutcliffe. Length of excitable knots. *Phys. Rev. E.*, 96:012218, 2017.
- J. C. Maxwell. *A Treatise on electricity and magnetism*. Cambridge: Cambridge University Press, 1873.
- N. D. Mermin. The topological theory of defects in ordered media. *Rev. Mod. Phys.*, 51:591–648, 1979.
- J. Milnor. *Topology from the differentiable viewpoint*. Princeton University Press, 1997.
- J. Milnor and J. D. Stasheff. *Characteristic classes*. Princeton university press, 1974.
- H. Moffatt. The degree of knottedness of tangled vortex lines. *JFM*, 35:117–129, 1969.
- H. K. Moffatt. Helicity and singular structures in fluid dynamics. *PNAS*, 111:3663–3700, 2014.
- H. K. Moffatt and R. L. Ricca. Helicity and the călugăreanu invariant. *Proc. R. Soc. A*, 439:411–429, 1992.
- J. J. Moreau. Constantes d'un lot tourbillonnaire en fluide parfait barotrope. *R. R. Acad. Sci. Paris*, 252:2810–2812, 1961.
- J. Nagumo, S. Arimoto, and S. Yoshizawa. An active pulse transmission line simulating nerve axon. *Biophys. J.*, 50:2061–2070, 1962.
- J. Prost P. G. de Gennes. *The Physics of Liquid Crystals*. Oxford Science Publications, 1996.
- R. L. Ricca and B. Nipoti. Gauss' linking number revisited. *J. Knot Theory Ramifications*, 20:1325–1343, 2011.
- editor. S. J. Hogan. *Nonlinear Dynamics and Chaos: Where do we go from here?* IoP, London, 2002.
- P. G. Saffman. *Vortex Dynamics*. Cambridge: Cambridge University Press, 1992.

- M.W. Scheeler, D. Kleckner, D. Proment, G.L. Kindlmann, and W.T.M. Irvine. Helicity conservation by flow across scales in reconnecting vortex links and knots. *PNAS*, 111:15350, 2014.
- M.W. Scheeler, W. M van Rees, H. Kedia, D.Kleckner, and W.T.M. Irvine. Complete measurement of helicity and its dynamics in vortex tubes. *Science*, 357:487–491, 2016.
- J. Selinger. Interpretation of saddle-splay and the oseen-frank free energy in liquid crystals. 2019. URL <https://arxiv.org/abs/1901.06306>.
- P. M. Sutcliffe and A. T. Winfree. Stability of knots in excitable media. *Phys. Rev. E.*, 68:016218, 2003.
- P. G. Tait. On knots i. *Transactions of the Royal Society of Edinburgh*, 28:145–190, 1876.
- P. G. Tait. On knots ii. *Transactions of the Royal Society of Edinburgh*, 32:327–342, 1883.
- P. G. Tait. On knots iii. *Transactions of the Royal Society of Edinburgh*, 32:493–506, 1884.
- M. Tasinkevych, M. G. Campbell, and I. I. Smalyukh. Splitting, linking, knotting, and solitonic escape of topological defects in nematic drops with handles. *Proc. Natl. Acad. Sci. USA*, 111:16268–16273, 2014.
- W. Thomson. On vortex atoms. *Proceedings of the Royal Society of Edinburgh*, 6: 94–105, 1867.
- U Tkalec, M. Ravnik, S. Čopar, S. Žumer, and I. Muševič. Reconfigurable knots and links in chiral nematic colloids. *Science*, 333:62–65, 2011.
- Jan Frederik Totz, Harald Engel, and Oliver Steinbock. Spatial confinement causes lifetime enhancement and expansion of vortex rings with positive filament tension. *New Journal of Physics*, 17:093043, 2015.
- J L Trueba and M Arrayás. Vorticity field, helicity integral and persistence of entanglement in reaction-diffusion systems. *J. Phys. A: Mathematical and Theoretical*, 42:282001, 2009.
- L. Tu. *An introduction to manifolds*. Springer, 2010.
- B. A. Khesin V. I. Arnold. *Topological methods in hydrodynamics*. Springer, 1999.

- S. Čopar, U. Tkalec, I. Muševič, and S. Žumer. Knot theory realizations in nematic colloids. *Proc. Natl. Acad. Sci. USA*, 112:1675–1680, 2015.
- A. T. Winfree. *The geometry of biological time*. Springer, 2001.
- A.T. Winfree. Stable particle-like solutions to the nonlinear wave equations of three-dimensional excitable media. *SIAM Rev.*, 32:1–53, 1990.
- A.T. Winfree and S.H. Strogatz. Singular filaments organize chemical waves in three dimension: I. geometrically simple waves. *Physica D*, 8:35–49, 1983a.
- A.T. Winfree and S.H. Strogatz. Singular filaments organize chemical waves in three dimension: II. twisted waves. *Physica D*, 9:65–80, 1983b.
- A.T. Winfree and S.H. Strogatz. Singular filaments organize chemical waves in three dimension: III. knotted waves. *Physica D*, 9:333–345, 1983c.
- A.T. Winfree and S.H. Strogatz. Singular filaments organize chemical waves in three dimension: IV. wave taxonomy. *Physica D*, 13:221–233, 1984.
- L. Woltjer. A theorem on force-free magnetic fields. *PNAS*, 44:489–491, 1958.